STANDARDIZED CATCH PER UNIT EFFORT OF YELLOWFIN TUNA IN THE INDIAN OCEAN FOR THE EUROPEAN PURSE SEINE FLEET OPERATING ON FLOATING OBJECTS

Giancarlo M. Correa[1,✉], Jon Uranga[3], David M. Kaplan[2], Gorka Merino[3], and María Lourdes Ramos Alonso[4]

[1] AZTI, Marine Research, Basque Research and Technology Alliance (BRTA), Txatxarramendi ugartea z/g, 48395 Sukarrieta (Bizkaia), Spain
[2] MARBEC (Univ. Montpellier, CNRS, Ifremer, IRD), av. Jean Monnet, CS30171, 34203 Sète, France
[3] AZTI, Marine Research, Basque Research and Technology Alliance (BRTA), Herrera Kaia, Portualdea z/g, 20110 Pasaia (Gipuzkoa), Spain
[4] Instituto Español de Oceanografía, Centro Oceanográfico de Málaga, Puerto Pesquero, s/n Apdo., 29640, Fuengirola, Málaga, Spain

✉ Correspondence: Giancarlo M. Correa <gmoron@azti.es>

SUMMARY

Abundance indices for yellowfin tuna (Thunnus albacares) in the Indian Ocean were derived from the European purse seine CPUE series (2010-2022) for fishing operations made on floating objects (FOB). We used two modelling approaches for CPUE standardization: generalized linear mixed model (GLMM) and spatiotemporal GLMM model (st-GLMM). Moreover, for both modelling approaches, we implemented a hurdle method, which separates the probability of a positive set and the catch (kg) per set in different components. Then, we made predictions on a prediction grid for every time step (year-quarter). To calculate the standardized CPUE per time step, we aggregated the spatial predictions based on an area-weighting approach. The two standardized CPUE series were then compared to the nominal CPUE. To remove the effects of technological improvements and FOB density, several candidate variables were tested to be included as explanatory variables.

KEYWORDS

Catchability, Yellowfin tuna, Indian Ocean, catch, effort

1. Introduction

An abundance index is a key data input in stock assessment models that can inform fluctuations in population abundance or biomass (Magnusson and Hilborn, 2007). Typically, an abundance index is obtained from fishery-independent (e.g., scientific surveys) and dependent sources. For highly migratory and large pelagic fishes (e.g., tunas), performing a scientific survey is impractical given the large extent of their distribution, therefore fishery-dependent abundance indices such as catch per unit effort (CPUE) are primarily used (Hoyle et al., 2024).

Using nominal CPUE is inappropriate since it is normally biased due to the spatial heterogeneity of fish populations, environmental factors, the behavior of fishers, and features of fishing vessels (Wilberg et al., 2009). These factors may produce a disparity between the nominal CPUE and true population abundance trends. For this reason, a CPUE standardization process needs to be performed in order to remove the impact of external factors that can influence catch rates (Maunder and Punt, 2004).

The European (EU) tuna purse seine fishery operating in the Indian Ocean has experienced significant technological developments during the last years, which has increased their efficiency in locating and catching tunas (Torres-Irineo et al., 2014). The EU purse seine fleet is divided into two categories: 1) targeting free-swimming schools (FS), and 2) fishing around floating objects (LS). The latter category initially used natural objects (e.g., logs) that occurred naturally in the ocean; however, they now use artificial buoys known as fishing aggregating devices (a.k.a. FADs) with incorporated technology (e.g., satellite tracks, echo-sounders) (Lopez et al., 2014).

The EU purse seine fleet principally targets three tuna species: yellowfin (*Thunnus albacares*), bigeye (*Thunnus obesus*), and skipjack (*Katsuwonus pelamis*). Yellowfin tuna (YFT) is a fast-growing species widely distributed in the Indian Ocean. The largest catches come from latitudes between 30°S and 20°N, primarily from the western Indian Ocean, and peaks from November to June (Artetxe-Arrate et al., 2021). Based on the last stock assessment, YFT is considered overfished and subject to overfishing (Fu et al., 2021). The purse seine fishery is the main fishing gear operating on this stock, contributing to ~ 36% of the total YFT annual catch, followed by handline, gillnet, and longline fisheries. The purse seine LS type catches mostly juveniles while the purse seine FS does mostly on adults (Fu et al., 2021).

The assessment platform used in the last assessment of the YFT stock in 2021 (Fu et al., 2021) was Stock Synthesis (Methot and Wetzel, 2013). The final configuration was spatially explicit with four areas and employed four indices of abundance to inform biomass trend over time per area derived from the long-line fishery. One of the indices presented during the assessment process was developed using information from the EU purse seine operating on free schools (Guery et al., 2021), which principally informed variations in YFT adult abundance. In this study, we use data from the EU purse seine operating on floating objects (LS) and diverse modelling techniques to derive standardized CPUE indices that can inform juvenile abundance in the assessment process and help to improve the stock assessment model estimates.

2. Methods

2.1. Data

We used logbook data from the EU purse seine fleet (Spain and France) targeting tropical tunas and operating on floating objects in the Indian Ocean from 2010 to 2022. The logbook data sets are managed by the Tuna Observatory (Ob7) and the Spanish Institute of Oceanography (IEO) for the French and Spanish fleets, respectively. The raw logbook data (Level 0) produced by the skippers were corrected in terms of total catch per set to account for the difference between reported catch at sea and landed catch. Likewise, the species composition per set was corrected based on port size sampling and the T3 methodology (Pallarés and Hallier, 1997) to generate Level 1 logbook data set.

We excluded observations from fishing sets that operated in areas (1° × 1°) that were not fished for less than nine years during the studied period in order to retain areas constantly sampled. Figure 2 shows all the fishing sets used in the CPUE standardization process and Figure 4 the yearly variation in the number of sets in the data. Figure 1 shows the histogram of all the catch per set values, both in the original and log-transformed scale.

2.2. Spatial indicators

Using the observed data, we calculated six indicators to summarize the spatial behavior of the fleet during the studied period. Diverse spatial indicators have previously been used for fishery-dependent (Kaplan et al., 2021; Russo et al., 2013; Sosa-López and Manzo-Monroy, 2002) and independent (Woillez et al., 2009; Woillez et al., 2007) sources to increase the chance of picking up changes in critical fleet-related factors over time. We calculated the following spatial indicators, which were calculated by year-quarter:

1. *Clark-Evans*: It is an index of point spatial aggregation (Clark and Evans, 1954), here represented by fishing sets, and provides information on how spatially aggregated the fishing sets took place. Smaller values indicate higher spatial aggregation of fishing sets.
2. *Covered area* (km^2): Represents the spatial expansion of the fishing sets. It was calculated assuming that each fishing set has an area of influence of 1 km^2, and then calculating the spatial union of those areas.
3. *Center of gravity (lon)*: Indicates the longitude where the YFT catches per set were centered.
4. *Center of gravity (lat)*: Indicates the latitude where the YFT catches per set were centered.
5. *Moran's autocorrelation coefficient*: Measure of spatial autocorrelation (Gittleman and Kot, 1990), which considers the YFT catch information per fishing set.
6. *Gini coefficient*: It is a measure of inequality (Cowell, 2011) among YFT catch per fishing set.

2.3. Statistical models

We used two modelling approaches to standardize the observed catch rates: a traditional generalized linear mixed model (GLMM) and a spatiotemporal GLMM (st-GLMM). The main difference between both approaches is the treatment of the spatial and temporal effects (see below). For both cases, we used the two-part *delta* or *hurdle* approach (Aitchison, 1955), which models two components: 1) probability of a positive set (catch > 0), modelled as a binomial response, and 2) catch per set, which assumed a log-normal response.

2.3.1. Generalized linear mixed model (GLMM)

The GLMM approach is widely used for CPUE standardization. It extends the generalized linear model (GLM) approach by including random variables in the linear predictor, allowing the modelling of fixed and random effects simultaneously (Zuur et al., 2009). Time and space are usually modelled as random effects.

The studied area was stratified by using a spatial cluster approach to identify strata that best match the population structure (Ono et al., 2015). To find these strata, we applied a k-medoids algorithm (Kaufman and Rousseeuw, 1990) using the $1^\circ \times 1^\circ$ catch information averaged over time (i.e., mean CPUE). We then calculated the Euclidean distance between pairs of grids, considering the mean CPUE values but also the longitude and latitude information of the grids, and then ran the cluster analysis. Finally, we found the optimal number of clusters by using the average silhouette width method (Rousseeuw, 1987). The identified clusters were used as the *cluster* variable in the GLMM (see Table 1).

The GLMM model can be represented as:

$$\eta = g(\mu) = \mathbf{X}\boldsymbol{\beta} + \alpha + \epsilon \qquad (1)$$

Where η is the linear predictor. μ is either the expected probability of presence with a logit link function (g) for the first model component, or the YFT catch (tons) per set (only for positive values) with a log link function for the second model component. $\mathbf{X}$ is the design matrix of fixed effects, and $\boldsymbol{\beta}$ is a vector of estimated parameters. α is the random effect ($\alpha \sim N(0, \sigma_\alpha^2)$). ϵ represents the random error. We implemented the GLMM model (Equation 1) in R using the package *glmmTMB* (Brooks et al., 2017).

The first model component did not include any type of spatial effect, and treated the temporal effect by including $year + quarter$ as fixed effects and $(1|year:quarter)$ as random effects.The second model component included $year + quarter + cluster$ as fixed effects, and the interaction between year, quarter and cluster $(1|year:quarter:cluster)$ was modelled as random effect. Both model components included the effect of vessel as

random effect $(1|numbat)$. For other candidate variables (see Table 1), we performed an analysis of variance (likelihood ratio Chisquare) to evaluate their effect on the response variable and retained only the significant ones.

Once significant candidate variables were identified, we then used the *DHARMa* R package (Hartig, 2022) to evaluate the model residuals. Standard raw residuals are not always appropriate when using GLMM, and other types of residuals (e.g., Pearson, deviance residuals) are commonly used instead. *DHARMa* uses a simulation-based approach to create readily interpretable scaled (quantile) residuals for generalized linear mixed models. We analyzed two plots produced by *DHARMa*: 1) the QQ plot residuals, which detects overall deviations from the expected distribution, and 2) the residual vs. predicted plot, which detects trends in residuals along model predictions and simulation outliers.

2.3.2. Spatiotemporal generalized linear mixed model (st-GLMM)

Geostatistical generalized linear mixed effects models can account for unmeasured variables (e.g., population biomass) that cause observations (e.g., catch) to be correlated over space and time through random effects (Anderson et al., 2024). A Gaussian random field (GRF) is multidimensional spatial process, where the random effects that describe the spatial pattern follow a multinomial distribution with mean $\mu = [\mu(s_1), \ldots, \mu(s_n)]$ and spatially structured covariance matrix Σ (Blangiardo and Cameletti, 2015).

For CPUE standardization, the *VAST* (Thorson, 2019) and *R-INLA* (Lindgren and Rue, 2015) R packages have been used in previous studies for distinct fish stocks (Grüss et al., 2019; e.g., Zhou et al., 2019). Recently, Anderson et al. (2024) developed the *sdmTMB* R package that implements geostatistical spatial and spatiotemporal GLMMs in TMB (Kristensen et al., 2016) for model fitting such as done in *VAST*, but also provides a user-friendly interface, especially for users familiar with the *glmmTMB* package. For this reason, we decided to use *sdmTMB* to implement a spatiotemporal model for CPUE standardization.

sdmTMB approximates the GRF by relying on the Stochastic Partial Differential Equation (SPDE) approach using the Integrated Nested Laplace Approximation in *R-INLA* to reduce computational costs. The first step to using the SPDE approach is to construct the mesh, which was composed of triangles covering the studied area with a minimum allowed triangle edge length (*cutoff*) of 75 km (Figure 12). We assumed the spatial correlation is Matérn and bilinearly interpolated over the prediction grid (see below) using the values at the mesh vertices. Following Anderson et al. (2024), our model can be mathematically represented as:

$$\eta = g(\mu) = \mathbf{X\beta} + \omega_s + \varepsilon_{s,t} \qquad (2)$$

Where ω is the spatial random field (i.e., constant across time), which represents the effect of latent spatial variables that are not otherwise accounted for in the model:

$$\omega \sim MVN(0, \Sigma_\omega)$$

ε_t represents the latent spatiotemporal effects and are assumed to be iid (i.e., independent at each time step):

$$\varepsilon_t \sim MVN(0, \Sigma_\varepsilon)$$

Σ is the covariance matrix of the multivariate normal (MVN) distribution. The spatial and spatiotemporal terms were only included for the second model component. Since *sdmTMB* requires to have the same fixed and random effects in both model components, we included all the candidate variables for both components, as well as the effect of vessel as random effect $(1|numbat)$. The model time step was quarter.

To analyze the residuals, we computed the randomized quantile residuals, also known as probability-integral-transform (PIT) residuals. (Dunn and Smyth, 1996). They apply randomization to integer response values, transform the residuals using the distribution function to reflect a uniform(0, 1) distribution, and transform those values such that they would be normal(0, 1) if consistent with the model (Anderson et al., 2024).

2.4. Standardized CPUE calculation

We calculated two standardized CPUE indices by year-quarter for each modelling approach (Equation 1, Equation 2). To do so, we made predictions ($\hat{.}$) on the response scale for each model component for all combinations

of years y, quarters q, and areas a. The area a represents a cluster for the GLMM or a $1^\circ \times 1^\circ$ prediction grid for the st-GLMM model (Figure 3). For other covariates, we assumed the mean value of the continuous covariates, or the level with the largest sample size for discrete covariates.

Then, the predicted values of both model components were multiplied to produce the CPUE per year, quarter, and area ($\widehat{CPUE}_{y,q,a} = \hat{p}_{y,q,a}\hat{d}_{y,q,a}$), where $\hat{p}$ and $\hat{d}$ are the predictions for the first and second model component, respectively. Finally, we calculated the area-weighted CPUE by year-quarter:

$$\widehat{CPUE}_{y,q} = \sum_a A_a \times \widehat{CPUE}_{y,q,a} \qquad (3)$$

Where A_a is the area (km^2) of a, excluding the area on land. The estimates of abundance indices and their confidence intervals were then scaled to a mean of 1.

2.5. Uncertainty calculation

The standard error ($SE(.)$) of predictions was approximated based on Taylor expansion for each model component. For the first model component:

$$SE(\hat{p}) \approx \frac{exp(-\hat{\eta})}{\left(1 + exp(-\hat{\eta})\right)^2} SE(\hat{\eta})$$

Where $\hat{\eta}$ represents the predictions in the linear predictor scale (logit). For the second model component, we used:

$$SE\left(\hat{d}\right) \approx exp(\hat{\eta})SE(\hat{\eta})$$

Where $\hat{\eta}$ represents the predictions in linear predictor scale (log).

Then, we applied the delta-method (Lo et al., 1992) to calculate the standard error of the predicted CPUE ($\widehat{CPUE}$):

$$SE\left(\widehat{CPUE}\right) = \sqrt{SE(\hat{p})^2\hat{d}^2 + SE\left(\hat{d}\right)^2\hat{p}^2 + SE(\hat{p})^2 SE\left(\hat{d}\right)^2}$$

Finally, we compared the temporal trends of the standardized indices of abundance with the vulnerable biomass to the PS log-school fleet estimated in the last assessment model (Fu et al., 2021), which did not include any PS index of abundance. This was done only from 2010 and for the area 1b, which is the area where is fleet mainly operates.

3. Results

The number of sets included in our models increased from 2010 to 2018, and decreased since then (Figure 4). The values of catch per set were skewed to the left, with values generally smaller than 10 tons and rarely above 100 tonnes. In log-scale, we did not notice a clear temporal trend, but fluctuations over the years. Moreover, the proportion of null sets ranged from ~ 5% in 2016 to ~ 10% in 2020.

The fishing sets were more frequent in the western Indian Ocean, around the equator and areas close to Kenya and Somalia (Figure 6). On the other hand, catches were larger between 0 and 10°N (Figure 7). We did not observe a clear spatial pattern of areas with a high proportion of null sets (Figure 8).

3.1. Spatial indicators

We noticed that the covered area expanded progressively over the years until 2018, and then contracted and remained stable until 2022 (Figure 5). The Clark-Evans indices suggest that fishing set locations tended to be slightly more aggregated from 2010 to 2018, and then the level of aggregation decreased until 2022. The center of gravity (longitude) moved progressively from 53°E to 56°E over the years. In terms of latitude, the center of gravity moved from 2°S to 1°N. The Moran index indicated that the catch per set values slightly decreased their spatial

autocorrelation over the years. Moreover, the Gini index indicated that the catch per set values tended to be more heterogeneous from 2015 to 2022.

3.2. GLMM

The clustering method identified three optimal clusters in the studied area (Figure 9), which were included as the *cluster* variable in the GLMM model. When testing different candidate variables, we found that *num_buoys_20nm*, *num_owned_250km*, and *avg_density* variables were significant for model component 1 and *follow*, *country*, *num_buoys_20nm*, and *num_owned_250km* were significant for model component 2 (Table 2). When analyzing the residuals of the final model, we noted that there were no large deviations from the expected distribution, although the dispersion and outlier test were found significant (Figure 10). The simulated residuals did not show trends over model predictions. Using our final model, we then predicted CPUE by year, quarter, and cluster. Figure 11 shows these predictions averaged by year and cluster.

3.3. st-GLMM

The residual pattern for the first model component followed the assumed distribution quite well, while we observed a small tail of negative residuals for the second model component (Figure 13). The spatial patterns of residuals of component 2 did not show evident clustering of negative or positive residuals (Figure 14), which suggests that the model accounted for the spatial autocorrelation successfully. The spatial term of the model (ω) showed larger values in areas closer to the coast, and smaller values in offshore zones (Figure 15). Figure 16 shows the spatiotemporal term for each time step in the model. We then predicted CPUE by year, quarter, and grid in the prediction area (Figure 3), which were then averaged by year and grid (Figure 17). We noticed larger values in the north of the prediction area, especially during 2013 and 2022.

Figure 18 shows the standardized CPUE for both models (see Equation 3) and the nominal CPUE calculated as the average observed CPUE by time step (i.e., quarter). We observed similar standardized CPUE values for most time steps; however, larger differences were observed in 2013 and after 2019 between the GLMM and st-GLMM models. Also, the confidence interval for the st-GLMM model was larger than the GLMM model. There is a notable increase in standardized CPUE values from 2020 to 2022, especially for the st-GLMM. When comparing the standardized CPUEs with the vulnerable biomass, we noticed that their trends match quite well from 2010 to 2020, although a lag seemed to appear during 2017-2018 (Figure 19).

4. Discussion

In this study, we used two modelling approaches to standardize the CPUE of the European purse seine fleet operating on floating objects (FOB) in the Indian Ocean. The main difference in standardized CPUE between the two modelling approaches was observed in a couple of years (e.g., 2013 and after 2019). This difference was primarily produced by the quite high values predicted by the st-GLMM model in the northern area of the prediction grid. There is evidence that spatiotemporal models like the one implemented here (st-GLMM) outperform other approaches (Grüss et al., 2019), although the treatment of the space-time interaction in the GLMM approach should also perform adequately (Grüss et al., 2019; Ono et al., 2015). The use of spatiotemporal models has shown potential for CPUE standardization for tropical tunas using purse seine data operating on FOB (Castillo-Jordan et al., 2022; Xu and Lennert-Cody, 2022) and similar fisheries (Xu et al., 2019) in the Pacific Ocean.

Although not used in the last stock assessment model, Guery et al. (2021) also performed a standardization for the EU purse seine fleet operating on FOBs using a GLMM approach. In that study, a $5 \times 5^{\circ}$ grid factor was included as a fixed effect in the model, but there was no space-time interaction. One of the major improvements presented in this paper is the inclusion of the echosounder capacity of the buoys, which has been shown to increase the fishing power of this fleet (Wain et al., 2021). Also, we tested other variables related to the density of buoys, which were significant for both model components. One variable that might be included in future standardizations is the number of days at sea of the buoy on which the fishing set was performed. Previous evidence shows that tuna colonize FOBs the first 5-15 days after the FOB release in the ocean (Orue et al., 2019), although it could be earlier and quite variable in some cases, especially in the Indian Ocean (Baidai et al., 2020).

We consider that the standardized indices presented here could be included in the stock assessment model for yellowfin to inform changes in the juvenile abundance, especially in the west Indian Ocean. The comparison of the CPUE trends with the vulnerable biomass from the last assessment matched quite well. The two indices derived from both modelling approaches could be tested in the assessment model, and the final index could be chosen based on statistical indicators (e.g., assessment model likelihood). However, if only one index needs to be chosen, we recommend using the st-GLMM index since the spatiotemporal modelling approach is supported by previous evidence and provides more realistic uncertainty. Finally, we recommend accounting for effort creep, which is particularly important for purse seine fisheries (Hoyle, 2024), during the assessment model implementation since there are factors that were not accounted for in this standardization.

5. References

Aitchison, J., 1955. On the Distribution of a Positive Random Variable Having a Discrete Probability Mass at the Origin. Journal of the American Statistical Association 50, 901. https://doi.org/10.2307/2281175

Anderson, S.C., Ward, E.J., English, P.A., Barnett, L.A.K., Thorson, J.T., 2024. sdmTMB: An R package for fast, flexible, and user-friendly generalized linear mixed effects models with spatial and spatiotemporal random fields. bioRxiv : the preprint server for biology. https://doi.org/10.1101/2022.03.24.485545

Artetxe-Arrate, I., Fraile, I., Marsac, F., Farley, J.H., Rodriguez-Ezpeleta, N., Davies, C.R., Clear, N.P., Grewe, P., Murua, H., 2021. A review of the fisheries, life history and stock structure of tropical tuna (skipjack Katsuwonus pelamis, yellowfin Thunnus albacares and bigeye Thunnus obesus) in the Indian Ocean, in: Advances in Marine Biology. Elsevier, pp. 39–89. https://doi.org/10.1016/bs.amb.2020.09.002

Baidai, Y., Dagorn, L., Amandè, M.J., Gaertner, D., Capello, M., 2020. Tuna aggregation dynamics at Drifting Fish Aggregating Devices: A view through the eyes of commercial echosounder buoys. ICES Journal of Marine Science 77, 2960–2970. https://doi.org/10.1093/icesjms/fsaa178

Blangiardo, M., Cameletti, M., 2015. Spatial and spatio-temporal Bayesian models with R-INLA. John Wiley and Sons, Inc, Chichester, West Sussex.

Brooks, M., E., Kristensen, K., Benthem, van, J., Magnusson, A., Berg, C., W., Nielsen, A., Skaug, H., J., Mächler, M., Bolker, B., M., 2017. glmmTMB Balances Speed and Flexibility Among Packages for Zero-inflated Generalized Linear Mixed Modeling. The R Journal 9, 378. https://doi.org/10.32614/RJ-2017-066

Castillo-Jordan, C., Teears, T., Hampton, J., Davies, N., Scutt Phillips, J., McKechnie, S., Peatman, T., Macdonald, J., Day, J., Magnusson, A., Scott, R., Scott, F., Pilling, G., Hamer, P., 2022. Stock assessment of skipjack tuna in the western and central Pacific Ocean: 2022 (No. WCPFC-SC18-2022/SA-WP-01 (REV5)). Western and Central Pacific Fisheries Commission.

Clark, P.J., Evans, F.C., 1954. Distance to Nearest Neighbor as a Measure of Spatial Relationships in Populations. Ecology 35, 445–453. https://doi.org/10.2307/1931034

Cowell, F., 2011. Measuring Inequality. Oxford University Press. https://doi.org/10.1093/acprof:osobl/9780199594030.001.0001

Dunn, P.K., Smyth, G.K., 1996. Randomized Quantile Residuals. Journal of Computational and Graphical Statistics 5, 236–244. https://doi.org/10.1080/10618600.1996.10474708

Fu, D., Urtizberea Ijurco, A., Cardinale, M., Methot, R.D., Hoyle, S.D., Merino, G., 2021. Preliminary Indian Yellowfin tuna stock assessment 1950-2020 (Stock Synthesis) (No. IOTC-2021-WPTT23-12). Indian Ocean Tuna Comission.

Gittleman, J.L., Kot, M., 1990. Adaptation: Statistics and a Null Model for Estimating Phylogenetic Effects. Systematic Zoology 39, 227. https://doi.org/10.2307/2992183

Grüss, A., Walter, J.F., Babcock, E.A., Forrestal, F.C., Thorson, J.T., Lauretta, M.V., Schirripa, M.J., 2019. Evaluation of the impacts of different treatments of spatio-temporal variation in catch-per-unit-effort standardization models. Fisheries Research 213, 75–93. https://doi.org/10.1016/j.fishres.2019.01.008

Guery, L., Kaplan, D., Marsac, F., Grande, M., Abascal, F., Baez, J.C., Gaertner, D., 2021. Standardized purse seine CPUE of Yellowfin tuna in the Indian Ocean for the European fleet (No. IOTC-2021-WPTT23-10). Indian Ocean Tuna Comission.

Hartig, F., 2022. DHARMa: Residual Diagnostics for Hierarchical (Multi-Level / Mixed) Regression Models.

Hoyle, S.D., 2024. Effort creep in longline and purse seine CPUE and its application in tropical tuna assessments (No. IOTC-2024-WPTT26(DP)-16). Indian Ocean Tuna Comission.

Hoyle, S.D., Campbell, R.A., Ducharme-Barth, N.D., Grüss, A., Moore, B.R., Thorson, J.T., Tremblay-Boyer, L., Winker, H., Zhou, S., Maunder, M.N., 2024. Catch per unit effort modelling for stock assessment: A summary of good practices. Fisheries Research 269, 106860. https://doi.org/10.1016/j.fishres.2023.106860

Kaplan, D., Baez, J.C., Pascual, P., Vidal, T., 2021. Temporal trends and variability in the spatial distribution of European tropical tuna purse-seine fishing in the Atlantic and Indian Oceans (No. IOTC-2021-WPTT23-20_Rev1). Indian Ocean Tuna Comission.

Kaufman, L., Rousseeuw, P.J., 1990. Finding groups in data: An introduction to cluster analysis, Wiley series in probability and mathematical statistics. Wiley, New York.

Kristensen, K., Nielsen, A., Berg, C.W., Skaug, H., Bell, B.M., 2016. TMB: Automatic Differentiation and Laplace Approximation. Journal of Statistical Software 70. https://doi.org/10.18637/jss.v070.i05

Lindgren, F., Rue, H., 2015. Bayesian Spatial Modelling with *R* - **INLA**. Journal of Statistical Software 63. https://doi.org/10.18637/jss.v063.i19

Lo, N.C., Jacobson, L.D., Squire, J.L., 1992. Indices of Relative Abundance from Fish Spotter Data based on Delta-Lognormal Models. Canadian Journal of Fisheries and Aquatic Sciences 49. https://doi.org/10.1139/f92-278

Lopez, J., Moreno, G., Sancristobal, I., Murua, J., 2014. Evolution and current state of the technology of echo-sounder buoys used by Spanish tropical tuna purse seiners in the Atlantic, Indian and Pacific Oceans. Fisheries Research 155, 127–137. https://doi.org/10.1016/j.fishres.2014.02.033

Magnusson, A., Hilborn, R., 2007. What makes fisheries data informative? Fish and Fisheries 8, 337–358. https://doi.org/10.1111/j.1467-2979.2007.00258.x

Maunder, M.N., Punt, A.E., 2004. Standardizing catch and effort data: A review of recent approaches. Fisheries Research 70, 141–159. https://doi.org/10.1016/j.fishres.2004.08.002

Methot, R.D., Wetzel, C.R., 2013. Stock synthesis: A biological and statistical framework for fish stock assessment and fishery management. Fisheries Research 142, 86–99. https://doi.org/10.1016/j.fishres.2012.10.012

Ono, K., Punt, A.E., Hilborn, R., 2015. Think outside the grids: An objective approach to define spatial strata for catch and effort analysis. Fisheries Research 170, 89–101. https://doi.org/10.1016/j.fishres.2015.05.021

Orue, B., Lopez, J., Moreno, G., Santiago, J., Soto, M., Murua, H., 2019. Aggregation process of drifting fish aggregating devices (DFADs) in the Western Indian Ocean: Who arrives first, tuna or non-tuna species? PLOS ONE 14, e0210435. https://doi.org/10.1371/journal.pone.0210435

Pallarés, P., Hallier, J.P., 1997. Analyse du schéma d'échantillonnage multispécifique des thonidés tropicaux (Rapport Scientifique No. OEP/ORSTOM, Programme n° 95/37 réalisé avec le soutien financier de la Commission des Communautés Européennes). Madrid, Spain.

Rousseeuw, P.J., 1987. Silhouettes: A graphical aid to the interpretation and validation of cluster analysis. Journal of Computational and Applied Mathematics 20, 53–65. https://doi.org/10.1016/0377-0427(87)90125-7

Russo, T., Parisi, A., Cataudella, S., 2013. Spatial indicators of fishing pressure: Preliminary analyses and possible developments. Ecological Indicators 26, 141–153. https://doi.org/10.1016/j.ecolind.2012.11.002

Sosa-López, A., Manzo-Monroy, H., 2002. Spatial patterns of the yellowfin tuna (Thunnus albacares) in the Eastern Pacific Ocean: An exploration of concentration profiles. Ciencias Marinas 28, 331–346. https://doi.org/10.7773/cm.v28i4.241

Thorson, J.T., 2019. Guidance for decisions using the Vector Autoregressive Spatio-Temporal (VAST) package in stock, ecosystem, habitat and climate assessments. Fisheries Research 210, 143–161. https://doi.org/10.1016/j.fishres.2018.10.013

Torres-Irineo, E., Gaertner, D., Chassot, E., Dreyfus-León, M., 2014. Changes in fishing power and fishing strategies driven by new technologies: The case of tropical tuna purse seiners in the eastern Atlantic Ocean. Fisheries Research 155, 10–19. https://doi.org/10.1016/j.fishres.2014.02.017

Wain, G., Guéry, L., Kaplan, D.M., Gaertner, D., 2021. Quantifying the increase in fishing efficiency due to the use of drifting FADs equipped with echosounders in tropical tuna purse seine fisheries. ICES Journal of Marine Science 78, 235–245. https://doi.org/10.1093/icesjms/fsaa216

Wilberg, M.J., Thorson, J.T., Linton, B.C., Berkson, J., 2009. Incorporating Time-Varying Catchability into Population Dynamic Stock Assessment Models. Reviews in Fisheries Science 18, 7–24. https://doi.org/10.1080/10641260903294647

Woillez, M., Poulard, J.-C., Rivoirard, J., Petitgas, P., Bez, N., 2007. Indices for capturing spatial patterns and their evolution in time, with application to European hake (Merluccius merluccius) in the Bay of Biscay. ICES Journal of Marine Science 64, 537–550. https://doi.org/10.1093/icesjms/fsm025

Woillez, M., Rivoirard, J., Petitgas, P., 2009. Notes on survey-based spatial indicators for monitoring fish populations. Aquatic Living Resources 22, 155–164. https://doi.org/10.1051/alr/2009017

Xu, H., Lennert-Cody, C.E., 2022. Standardizing the purse-seine indices of abundance and associated length compositions for skipjack tuna in the eastern Pacific Ocean (No. SAC-13 INF-K). Inter-American Tropical Tuna Commission, La Jolla, CA.

Xu, H., Lennert-Cody, C.E., Maunder, M.N., Minte-Vera, C.V., 2019. Spatiotemporal dynamics of the dolphin-associated purse-seine fishery for yellowfin tuna (Thunnus albacares) in the eastern Pacific Ocean. Fisheries Research 213, 121–131. https://doi.org/10.1016/j.fishres.2019.01.013

Zhou, S., Campbell, R.A., Hoyle, S.D., 2019. Catch per unit effort standardization using spatio-temporal models for Australia's Eastern Tuna and Billfish Fishery. ICES Journal of Marine Science 76, 1489–1504. https://doi.org/10.1093/icesjms/fsz034

Zuur, A.F., Ieno, E.N., Walker, N., Saveliev, A.A., Smith, G.M., 2009. Mixed effects models and extensions in ecology with R, Statistics for Biology and Health. Springer New York, New York, NY. https://doi.org/10.1007/978-0-387-87458-6

6. Tables

Table 1: Candidate explanatory variables for the tested CPUE standardization models.

Variable code	Variable description	Variable type
year	Year	Factor (levels: 2010,…,2022)
quarter	Quarter of the year	Factor (levels: 1,2,3,4)
cluster	Clustered area (only for GLMM)	Factor (levels: 1,2,3,4)
lon	Longitude	Numeric
lat	Latitude	Numeric
time	Time as continuous (calculated from year and quarter values)	Numeric
country	Fleet country	Factor (levels: France, Spain)
numbat	Vessel identifier code	Factor (levels meaningless)
follow	Followed a FAD? It had echosounder capacity?	Factor (levels: No, Yes_No-Echo, Yes_Echo)
num_buoys_20nm	Number of buoys within 20 nm	Numeric
num_owned_250km	Number of owned buoys within 250 km	Numeric
avg_density	Monthly average density of buoys in a 1x1 grid	Numeric

Table 2: ANOVA analysis to identify significant fixed effects to be included in the GLMM model.

Component	Term	Chisq	DF	p.val
Component 1	year	54.63	12	<0.01
Component 1	quarter	62.78	3	<0.01
Component 1	country	0.55	1	0.46
Component 1	num_buoys_20nm	8.20	1	<0.01
Component 1	num_owned_250km	31.28	1	<0.01
Component 1	avg_density	5.33	1	0.02
Component 1	follow	3.11	2	0.21
Component 2	year	106.06	12	<0.01
Component 2	quarter	93.71	3	<0.01
Component 2	cluster	87.35	2	<0.01
Component 2	country	5.90	1	0.02
Component 2	num_buoys_20nm	12.42	1	<0.01
Component 2	num_owned_250km	45.17	1	<0.01
Component 2	avg_density	2.85	1	0.09
Component 2	follow	18.51	2	<0.01

Table 3: Summary of the GLMM model.

Component	Term	Est	Std.err	p.val
Component 1	(Intercept)	-2.534	0.131	<0.01
Component 1	year2011	0.004	0.154	0.98
Component 1	year2012	0.296	0.153	0.05
Component 1	year2013	-0.029	0.155	0.85
Component 1	year2014	0.121	0.152	0.43
Component 1	year2015	0.102	0.155	0.51
Component 1	year2016	-0.264	0.161	0.1
Component 1	year2017	0.136	0.157	0.39
Component 1	year2018	-0.174	0.156	0.27
Component 1	year2019	0.024	0.155	0.88
Component 1	year2020	0.539	0.151	<0.01
Component 1	year2021	-0.083	0.157	0.59
Component 1	year2022	-0.183	0.159	0.25
Component 1	quarter2	0.148	0.081	0.07
Component 1	quarter3	-0.446	0.081	<0.01
Component 1	quarter4	-0.289	0.080	<0.01
Component 1	num_buoys_20nm	0.003	0.001	0.01
Component 1	num_owned_250km	-0.009	0.002	<0.01
Component 1	avg_density	0.005	0.002	0.03
Component 1	sd__(Intercept)	0.163		
Component 1	sd__(Intercept)	0.309		
Component 2	(Intercept)	2.478	0.040	<0.01
Component 2	year2011	0.003	0.043	0.94
Component 2	year2012	-0.025	0.043	0.56
Component 2	year2013	0.113	0.043	0.01
Component 2	year2014	-0.045	0.043	0.3
Component 2	year2015	-0.162	0.043	<0.01
Component 2	year2016	-0.127	0.043	<0.01
Component 2	year2017	-0.073	0.043	0.09
Component 2	year2018	-0.024	0.042	0.56
Component 2	year2019	-0.181	0.042	<0.01
Component 2	year2020	-0.165	0.043	<0.01
Component 2	year2021	-0.105	0.042	0.01
Component 2	year2022	0.041	0.042	0.34
Component 2	quarter2	-0.130	0.024	<0.01
Component 2	quarter3	0.089	0.023	<0.01
Component 2	quarter4	0.061	0.022	0.01
Component 2	cluster2	-0.120	0.019	<0.01

Component 2	cluster3	0.073	0.021	<0.01
Component 2	countrySpain	0.058	0.024	0.01
Component 2	num_buoys_20nm	0.000	0.000	<0.01
Component 2	num_owned_250km	0.002	0.000	<0.01
Component 2	followYes_No-echo	-0.068	0.017	<0.01
Component 2	followYes_Echo	0.009	0.006	0.13
Component 2	sd__(Intercept)	0.090		
Component 2	sd__(Intercept)	0.068		

Table 4: Summary of the st-GLMM model.

Component	Term	Est	Std.err
Component 1	time_factor2010	2.283	0.150
Component 1	time_factor2010.25	2.876	0.252
Component 1	time_factor2010.5	2.892	0.156
Component 1	time_factor2010.75	2.709	0.161
Component 1	time_factor2011	2.092	0.150
Component 1	time_factor2011.25	2.181	0.201
Component 1	time_factor2011.5	3.112	0.166
Component 1	time_factor2011.75	3.052	0.161
Component 1	time_factor2012	2.383	0.171
Component 1	time_factor2012.25	1.852	0.160
Component 1	time_factor2012.5	2.885	0.171
Component 1	time_factor2012.75	2.177	0.146
Component 1	time_factor2013	2.474	0.160
Component 1	time_factor2013.25	2.529	0.204
Component 1	time_factor2013.5	2.588	0.143
Component 1	time_factor2013.75	2.982	0.156
Component 1	time_factor2014	2.368	0.139
Component 1	time_factor2014.25	2.019	0.145
Component 1	time_factor2014.5	2.954	0.152
Component 1	time_factor2014.75	2.540	0.141
Component 1	time_factor2015	2.253	0.159
Component 1	time_factor2015.25	1.980	0.162
Component 1	time_factor2015.5	2.932	0.165
Component 1	time_factor2015.75	2.777	0.144
Component 1	time_factor2016	2.534	0.158
Component 1	time_factor2016.25	2.472	0.168
Component 1	time_factor2016.5	3.132	0.164
Component 1	time_factor2016.75	3.315	0.180
Component 1	time_factor2017	2.560	0.159
Component 1	time_factor2017.25	2.415	0.154
Component 1	time_factor2017.5	2.774	0.153
Component 1	time_factor2017.75	2.093	0.146
Component 1	time_factor2018	2.669	0.141
Component 1	time_factor2018.25	2.578	0.157
Component 1	time_factor2018.5	3.062	0.160
Component 1	time_factor2018.75	2.720	0.156
Component 1	time_factor2019	2.136	0.134
Component 1	time_factor2019.25	2.331	0.160
Component 1	time_factor2019.5	3.064	0.166

Component 1	time_factor2019.75	2.783	0.149
Component 1	time_factor2020	2.137	0.130
Component 1	time_factor2020.25	1.804	0.142
Component 1	time_factor2020.5	1.938	0.136
Component 1	time_factor2020.75	2.262	0.137
Component 1	time_factor2021	2.692	0.166
Component 1	time_factor2021.25	2.305	0.135
Component 1	time_factor2021.5	2.910	0.162
Component 1	time_factor2021.75	2.772	0.173
Component 1	time_factor2022	2.798	0.165
Component 1	time_factor2022.25	2.316	0.151
Component 1	time_factor2022.5	3.010	0.165
Component 1	time_factor2022.75	2.967	0.204
Component 1	countrySpain	0.086	0.112
Component 1	num_buoys_20nm	-0.003	0.001
Component 1	num_owned_250km	0.009	0.002
Component 1	followYes_No-echo	-0.048	0.121
Component 1	followYes_Echo	0.072	0.043
Component 1	avg_density	-0.005	0.002
Component 2	time_factor2010	2.074	0.136
Component 2	time_factor2010.25	2.151	0.165
Component 2	time_factor2010.5	2.501	0.140
Component 2	time_factor2010.75	2.368	0.131
Component 2	time_factor2011	2.400	0.134
Component 2	time_factor2011.25	1.963	0.150
Component 2	time_factor2011.5	2.441	0.149
Component 2	time_factor2011.75	2.464	0.128
Component 2	time_factor2012	2.415	0.143
Component 2	time_factor2012.25	1.922	0.153
Component 2	time_factor2012.5	2.482	0.138
Component 2	time_factor2012.75	2.287	0.131
Component 2	time_factor2013	2.567	0.131
Component 2	time_factor2013.25	2.482	0.154
Component 2	time_factor2013.5	2.871	0.133
Component 2	time_factor2013.75	2.320	0.126
Component 2	time_factor2014	2.536	0.133
Component 2	time_factor2014.25	2.176	0.145
Component 2	time_factor2014.5	2.365	0.138
Component 2	time_factor2014.75	2.197	0.128
Component 2	time_factor2015	2.054	0.132
Component 2	time_factor2015.25	1.924	0.152
Component 2	time_factor2015.5	2.299	0.151

Component 2	time_factor2015.75	2.015	0.127
Component 2	time_factor2016	2.189	0.130
Component 2	time_factor2016.25	1.908	0.136
Component 2	time_factor2016.5	2.440	0.130
Component 2	time_factor2016.75	2.244	0.123
Component 2	time_factor2017	2.146	0.128
Component 2	time_factor2017.25	2.206	0.145
Component 2	time_factor2017.5	2.342	0.135
Component 2	time_factor2017.75	2.399	0.130
Component 2	time_factor2018	2.490	0.124
Component 2	time_factor2018.25	2.044	0.129
Component 2	time_factor2018.5	2.360	0.125
Component 2	time_factor2018.75	2.253	0.122
Component 2	time_factor2019	2.246	0.123
Component 2	time_factor2019.25	1.484	0.138
Component 2	time_factor2019.5	2.085	0.138
Component 2	time_factor2019.75	2.060	0.132
Component 2	time_factor2020	1.677	0.132
Component 2	time_factor2020.25	1.609	0.131
Component 2	time_factor2020.5	2.309	0.132
Component 2	time_factor2020.75	2.268	0.128
Component 2	time_factor2021	2.104	0.134
Component 2	time_factor2021.25	1.750	0.134
Component 2	time_factor2021.5	2.174	0.138
Component 2	time_factor2021.75	2.266	0.132
Component 2	time_factor2022	2.522	0.127
Component 2	time_factor2022.25	2.311	0.135
Component 2	time_factor2022.5	2.595	0.138
Component 2	time_factor2022.75	2.666	0.138
Component 2	countrySpain	0.042	0.047
Component 2	num_buoys_20nm	-0.002	0.000
Component 2	num_owned_250km	0.003	0.000
Component 2	followYes_No-echo	-0.115	0.031
Component 2	followYes_Echo	0.011	0.011
Component 2	avg_density	-0.003	0.001
Component 2	range	587.931	34.574
Component 2	phi	0.952	0.003
Component 2	sigma_O	0.169	0.015
Component 2	sigma_E	0.361	0.010
Component 2	sigma_G	0.135	0.018

Table 5: Predicted CPUE, 95% confidence interval, and standard error (SE) by the GLMM model by year and quarter (Time column).

Time	Est	Lower	Upper	SE
2010.00	0.94	0.85	1.02	0.04
2010.25	0.95	0.84	1.06	0.05
2010.50	1.18	1.11	1.24	0.03
2010.75	1.16	1.09	1.24	0.04
2011.00	1.01	0.93	1.09	0.04
2011.25	0.89	0.79	0.98	0.05
2011.50	1.16	1.10	1.23	0.03
2011.75	1.17	1.11	1.23	0.03
2012.00	1.05	0.95	1.15	0.05
2012.25	0.85	0.76	0.95	0.05
2012.50	1.11	1.03	1.18	0.04
2012.75	1.03	0.96	1.10	0.04
2013.00	1.15	1.06	1.23	0.04
2013.25	1.06	0.94	1.17	0.06
2013.50	1.37	1.29	1.44	0.04
2013.75	1.08	1.03	1.14	0.03
2014.00	1.12	1.04	1.20	0.04
2014.25	0.86	0.78	0.94	0.04
2014.50	1.06	1.00	1.13	0.03
2014.75	0.96	0.90	1.01	0.03
2015.00	0.88	0.82	0.95	0.03
2015.25	0.80	0.72	0.87	0.04
2015.50	0.96	0.90	1.02	0.03
2015.75	0.91	0.86	0.96	0.02
2016.00	0.93	0.87	0.99	0.03
2016.25	0.78	0.72	0.85	0.03
2016.50	1.05	0.99	1.10	0.03
2016.75	0.99	0.94	1.05	0.03
2017.00	0.91	0.85	0.97	0.03
2017.25	0.92	0.85	0.99	0.03
2017.50	1.02	0.96	1.07	0.03
2017.75	1.04	0.97	1.11	0.03
2018.00	1.14	1.08	1.19	0.03
2018.25	0.93	0.87	0.99	0.03
2018.50	1.10	1.05	1.15	0.03
2018.75	1.01	0.95	1.06	0.03
2019.00	0.90	0.85	0.96	0.03
2019.25	0.73	0.68	0.78	0.03
2019.50	0.95	0.89	1.00	0.03

2019.75	0.99	0.94	1.03	0.03
2020.00	0.81	0.76	0.87	0.03
2020.25	0.73	0.67	0.78	0.03
2020.50	1.01	0.95	1.08	0.03
2020.75	1.02	0.97	1.08	0.03
2021.00	0.93	0.87	0.99	0.03
2021.25	0.81	0.76	0.86	0.02
2021.50	1.04	0.99	1.10	0.03
2021.75	1.06	0.99	1.12	0.03
2022.00	1.09	1.03	1.15	0.03
2022.25	0.98	0.91	1.05	0.04
2022.50	1.17	1.11	1.23	0.03
2022.75	1.25	1.17	1.33	0.04

Table 6: Predicted CPUE, 95% confidence interval, and standard error (SE) by the st-GLMM model by year and quarter (Time column).

Time	Est	Lower	Upper	SE
2010.00	0.84	0.70	1.00	0.08
2010.25	0.93	0.75	1.17	0.11
2010.50	1.25	1.07	1.48	0.10
2010.75	1.23	1.03	1.47	0.11
2011.00	1.11	0.93	1.32	0.10
2011.25	0.70	0.57	0.86	0.07
2011.50	1.20	1.01	1.43	0.11
2011.75	1.26	1.09	1.46	0.09
2012.00	1.17	0.97	1.41	0.11
2012.25	0.64	0.53	0.77	0.06
2012.50	1.23	1.06	1.44	0.10
2012.75	0.93	0.79	1.10	0.08
2013.00	1.35	1.14	1.59	0.11
2013.25	1.22	1.00	1.48	0.12
2013.50	1.69	1.44	1.99	0.14
2013.75	1.16	1.01	1.34	0.08
2014.00	1.33	1.14	1.56	0.11
2014.25	0.82	0.69	0.97	0.07
2014.50	1.08	0.93	1.26	0.08
2014.75	0.95	0.81	1.11	0.08
2015.00	0.88	0.74	1.04	0.08
2015.25	0.73	0.60	0.88	0.07
2015.50	1.04	0.86	1.25	0.10
2015.75	0.80	0.69	0.93	0.06
2016.00	0.86	0.74	1.00	0.07
2016.25	0.69	0.58	0.81	0.06
2016.50	1.23	1.05	1.43	0.10
2016.75	0.96	0.84	1.11	0.07
2017.00	0.82	0.70	0.96	0.07
2017.25	0.86	0.72	1.02	0.08
2017.50	1.10	0.94	1.29	0.09
2017.75	1.05	0.89	1.22	0.08
2018.00	1.28	1.12	1.47	0.09
2018.25	0.87	0.74	1.01	0.07
2018.50	1.17	1.03	1.33	0.08
2018.75	1.04	0.90	1.21	0.08
2019.00	0.94	0.82	1.08	0.07
2019.25	0.45	0.38	0.53	0.04
2019.50	0.91	0.77	1.08	0.08

2019.75	0.85	0.74	0.99	0.06
2020.00	0.55	0.47	0.63	0.04
2020.25	0.44	0.38	0.50	0.03
2020.50	0.98	0.83	1.16	0.08
2020.75	0.88	0.75	1.03	0.07
2021.00	0.81	0.66	0.99	0.09
2021.25	0.58	0.49	0.69	0.05
2021.50	0.95	0.80	1.13	0.09
2021.75	0.97	0.83	1.15	0.08
2022.00	1.18	1.02	1.37	0.09
2022.25	0.99	0.81	1.20	0.10
2022.50	1.44	1.22	1.70	0.12
2022.75	1.62	1.36	1.94	0.15

7. Figures

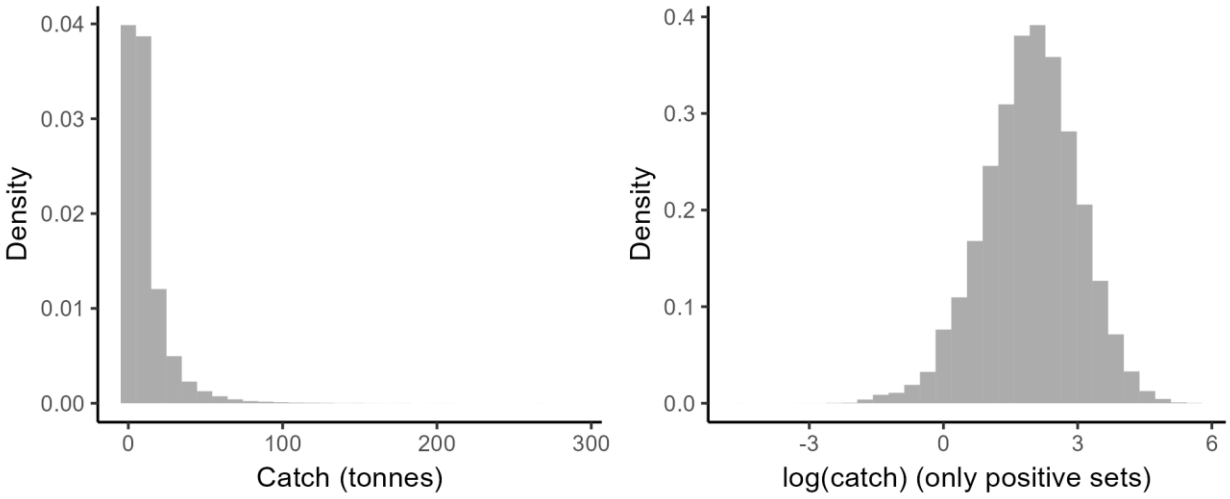

Figure 1: Distribution of observed catch per set values (only positive fishing sets).

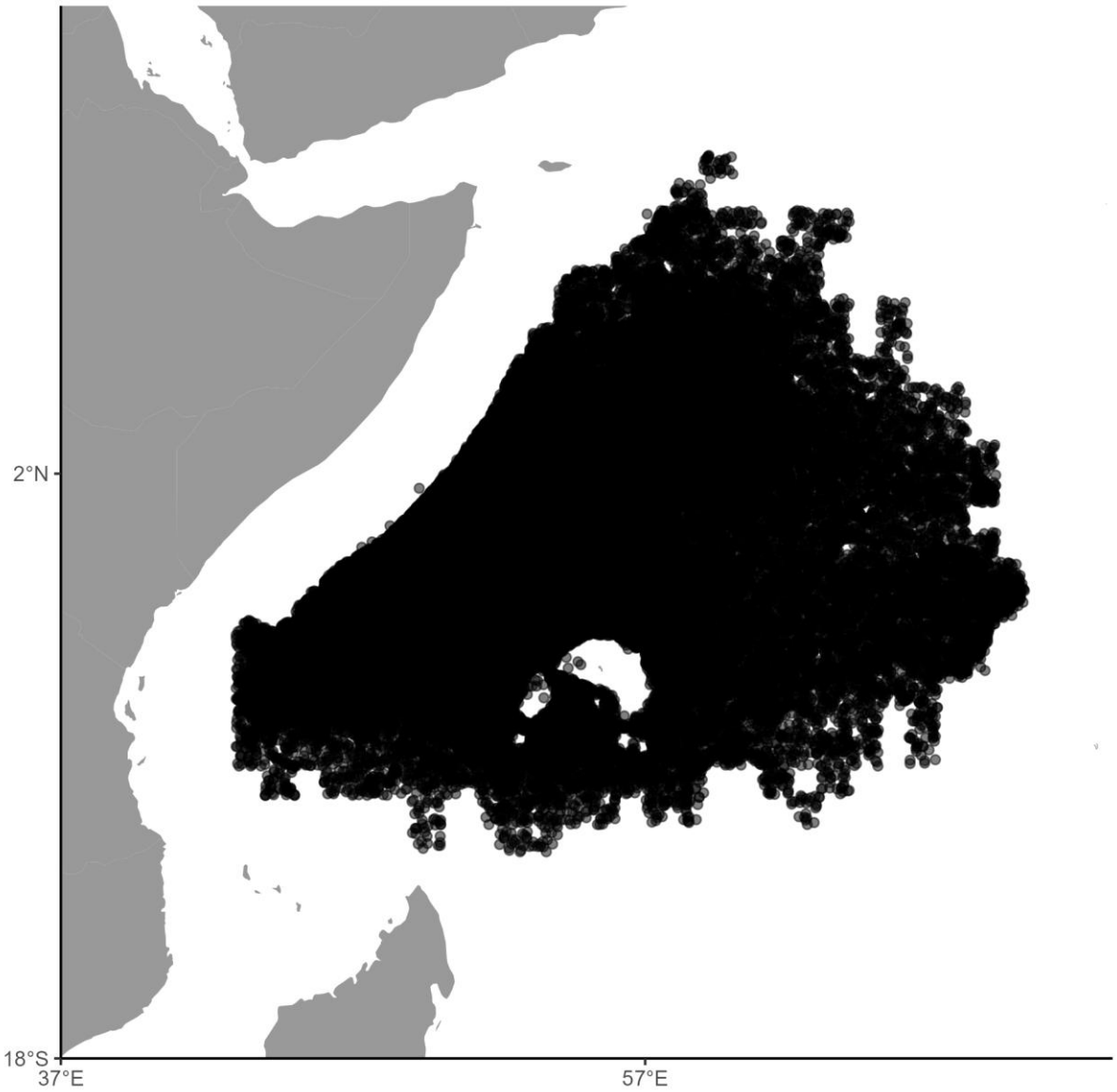

Figure 2: Fishing sets included in the standardization process.

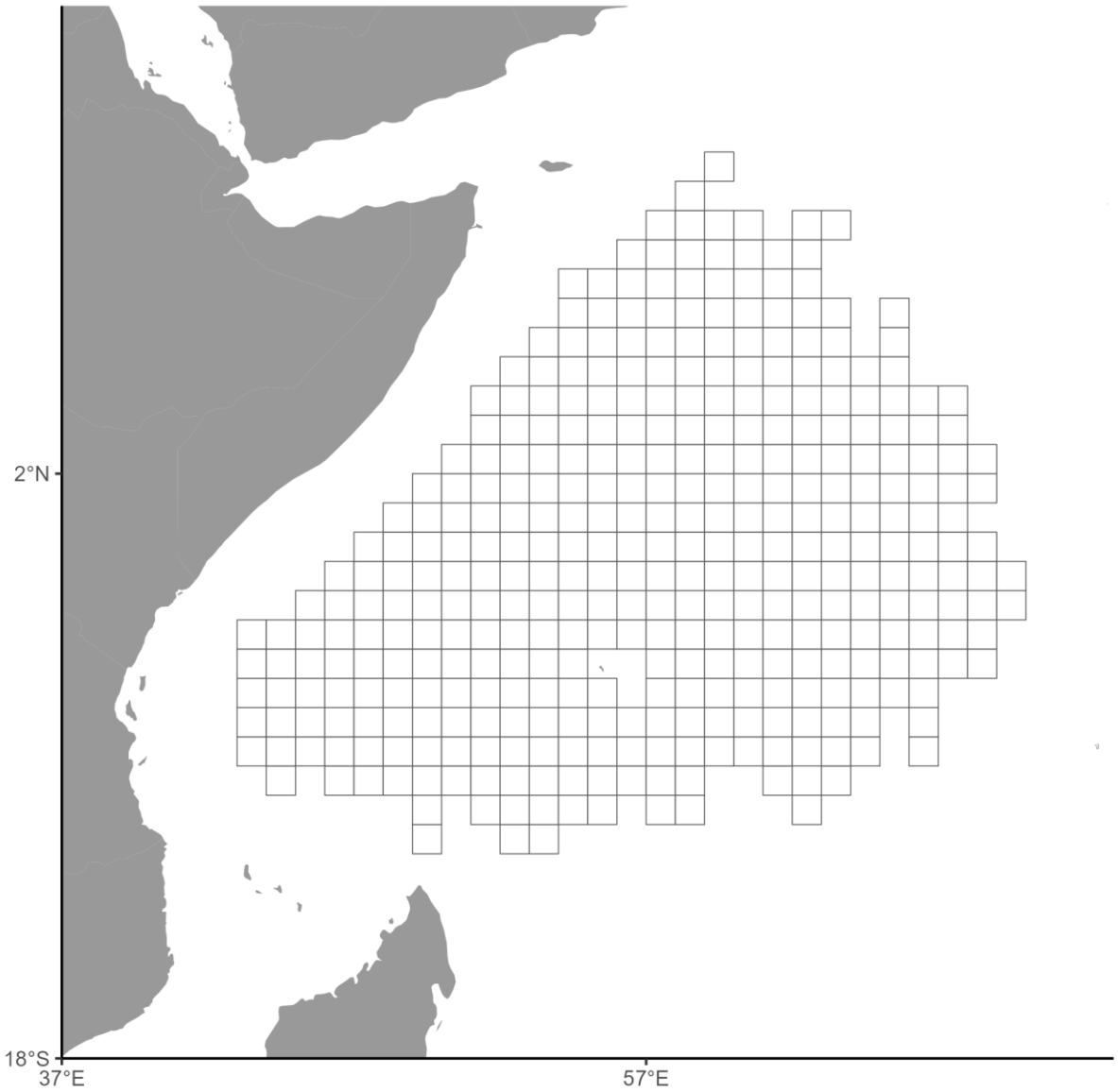

Figure 3: Prediction grid used for the st-GLMM model.

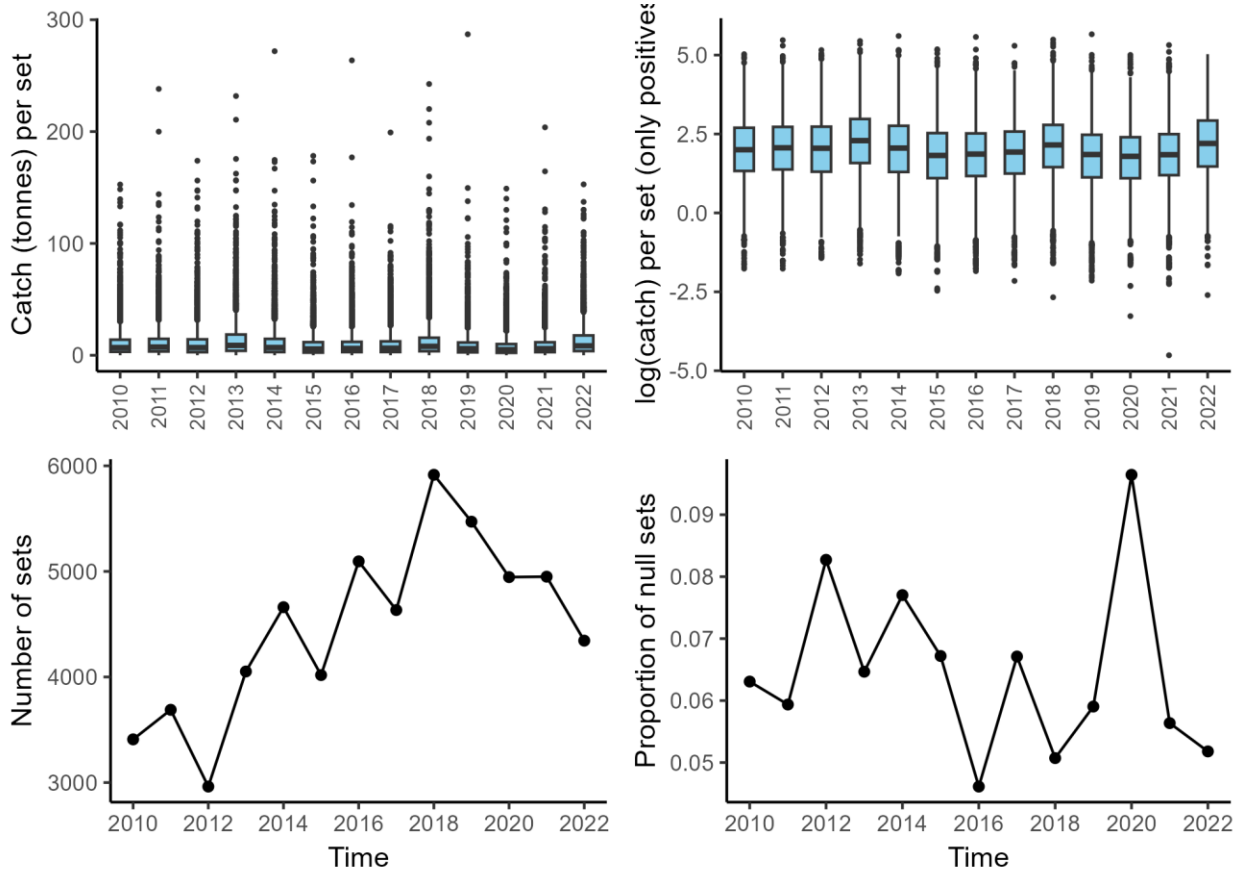

Figure 4: Distribution of catch per set, number of sets, and proportion of null sets in the data per year.

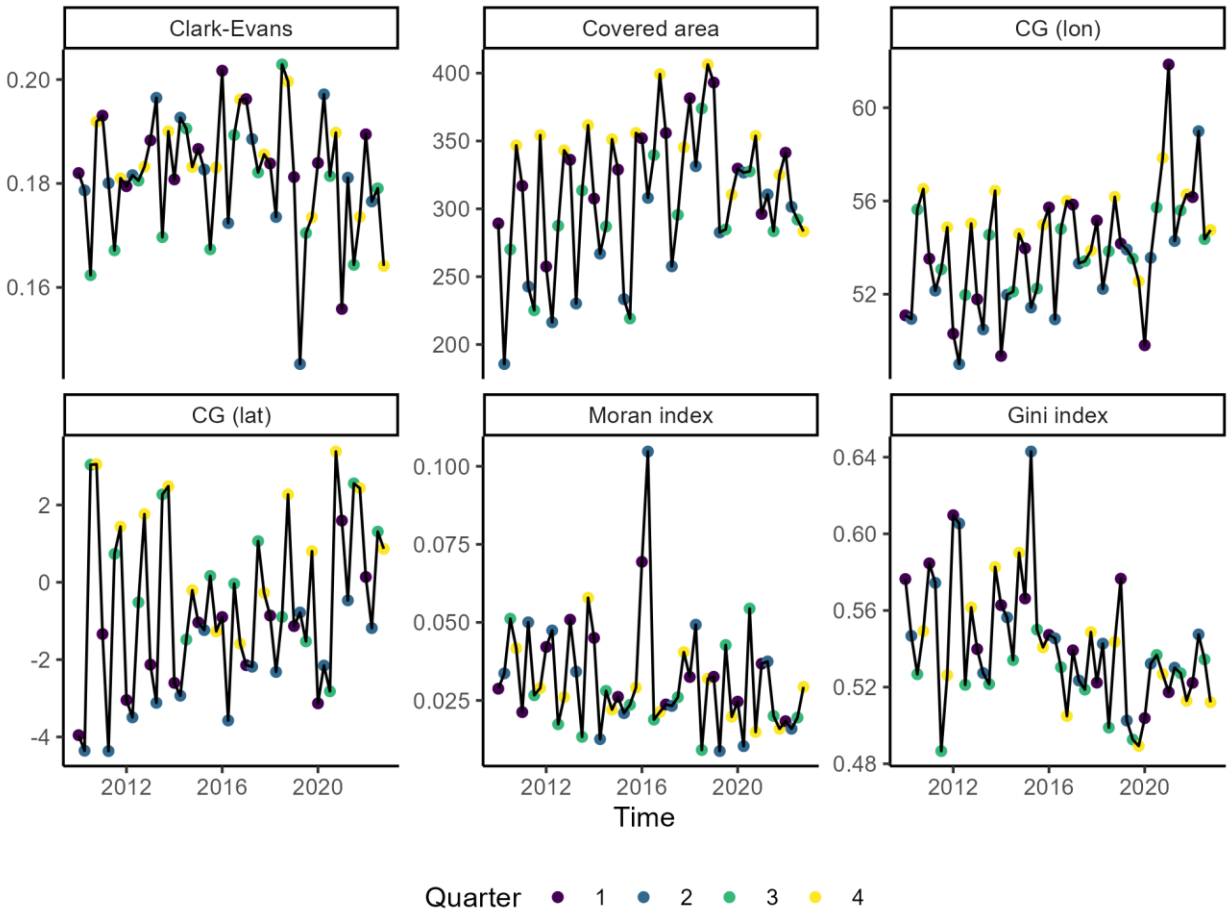

Figure 5: Spatial indicators calculated by year-quarter.

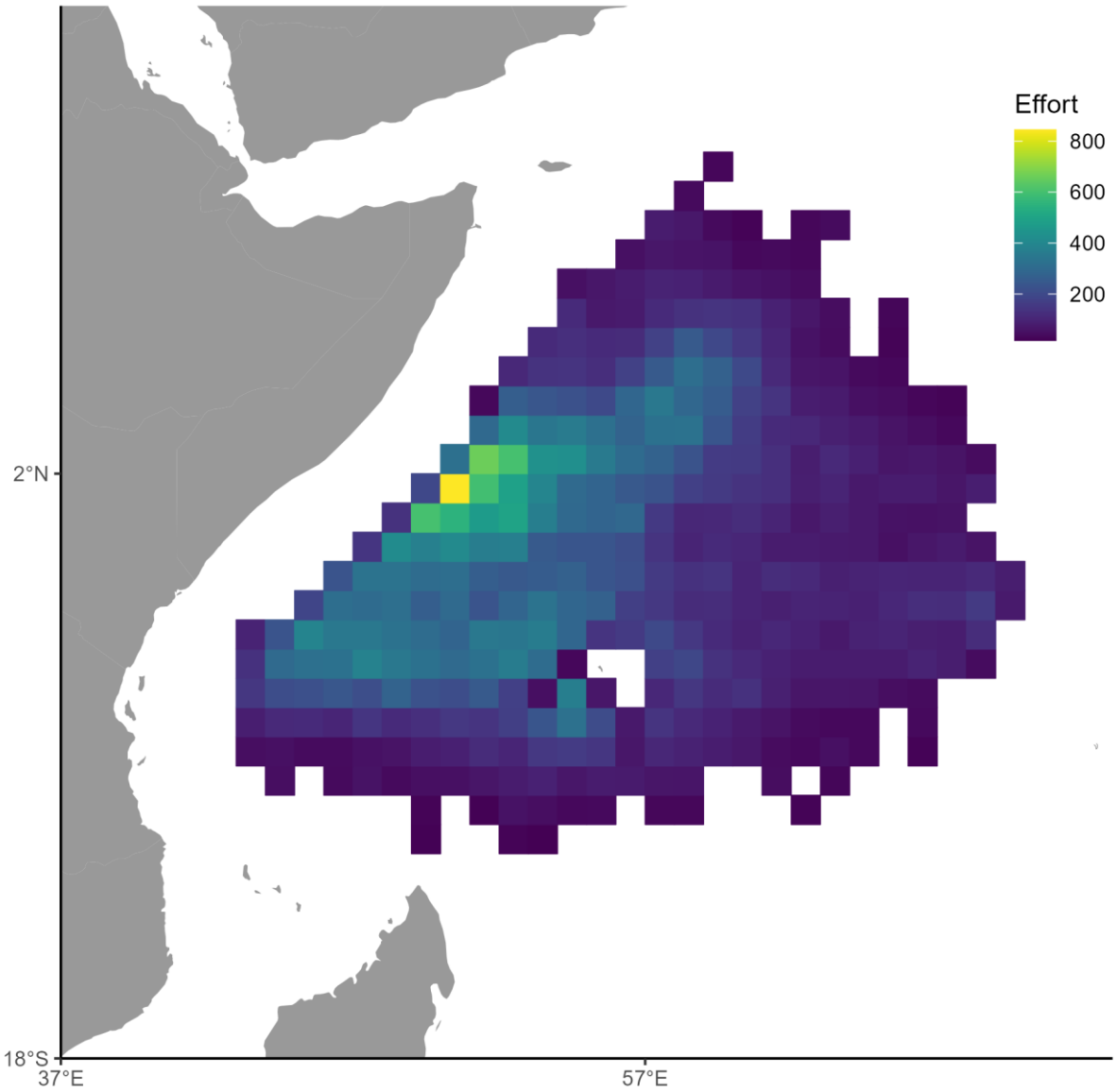

Figure 6: Aggregated number of fishing sets (effort) per grid.

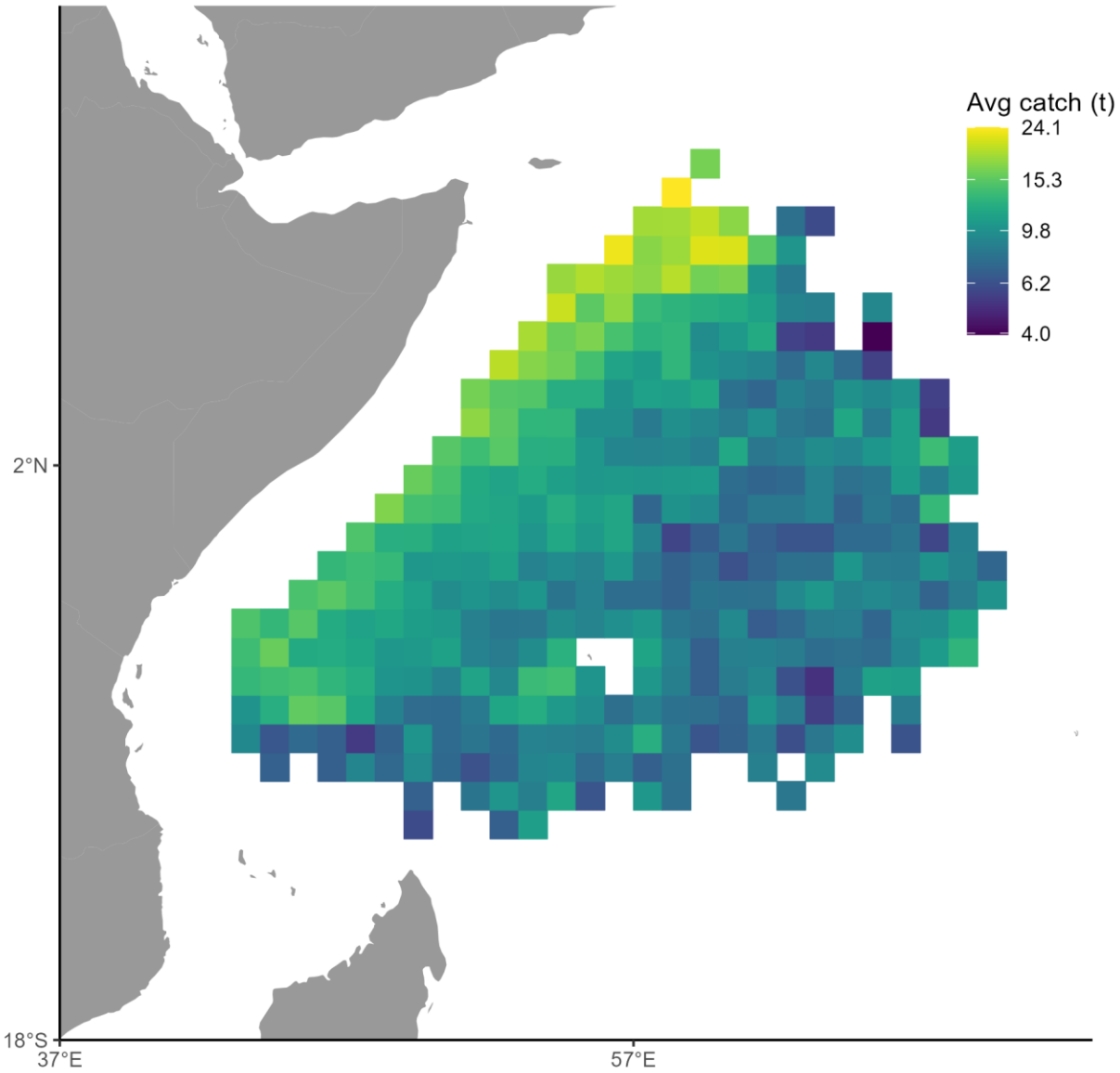

Figure 7: Average catch per grid.

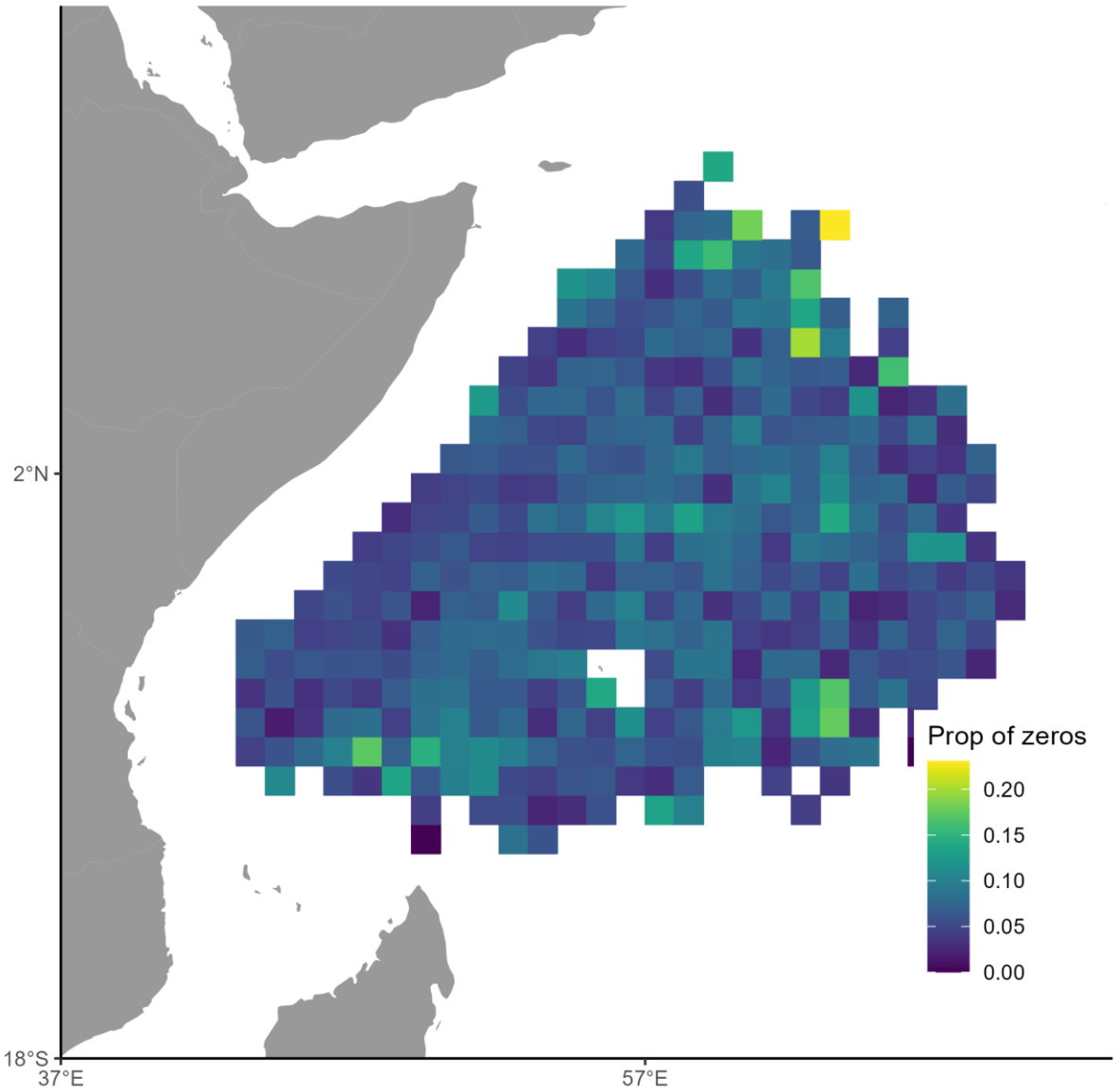

Figure 8: Proportion of null sets per grid.

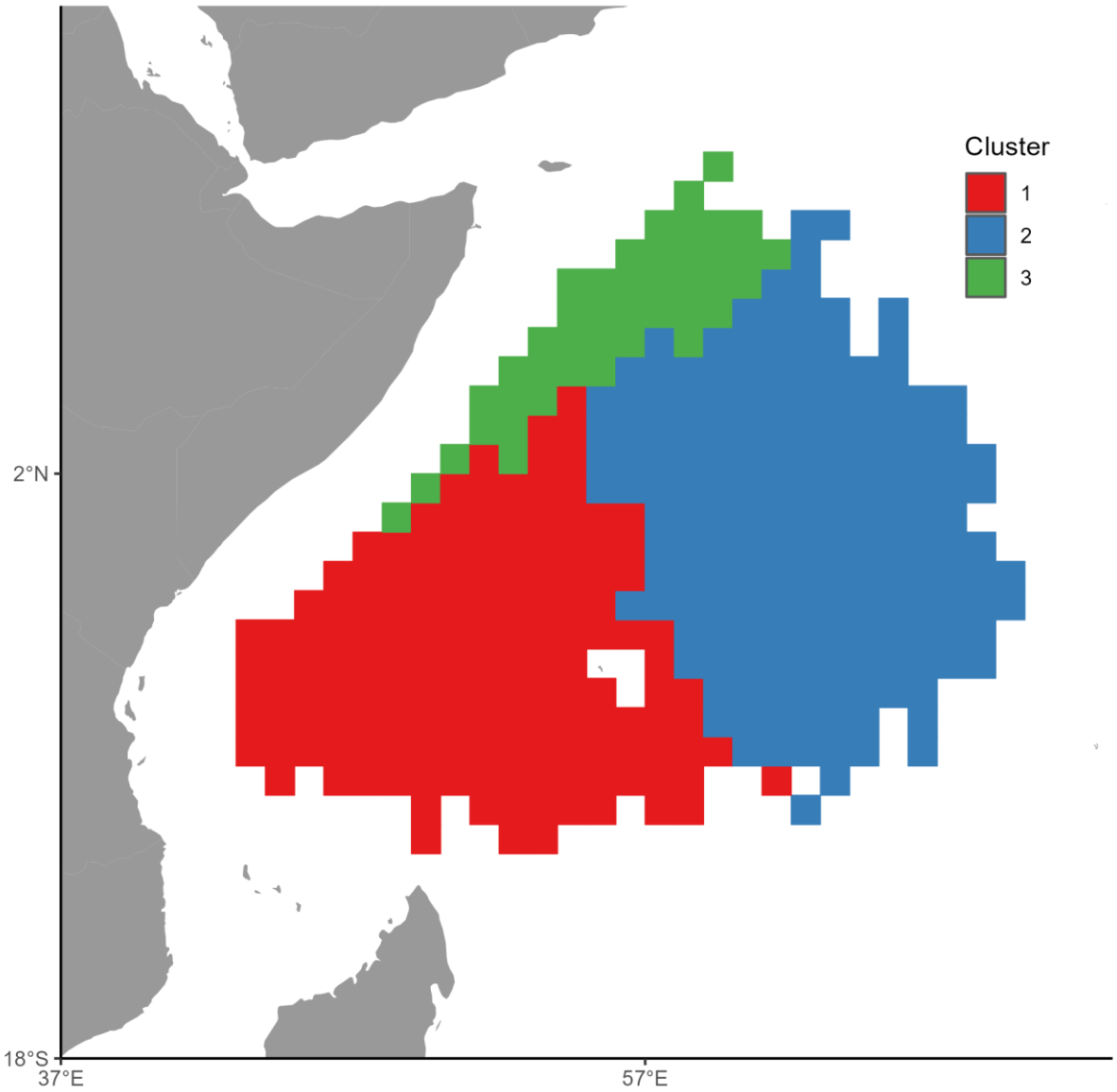

Figure 9: Strata identified by the clustering method and used in the GLMM (*cluster* variable).

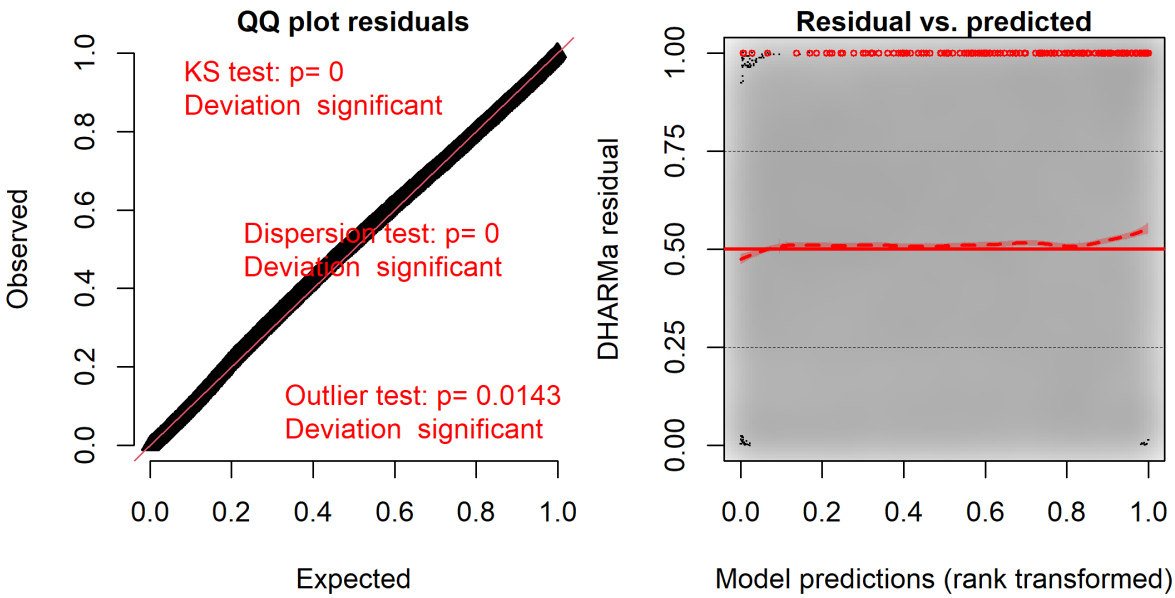

Figure 10: QQ-plot (left) and residual plot (right) for the GLMM model.

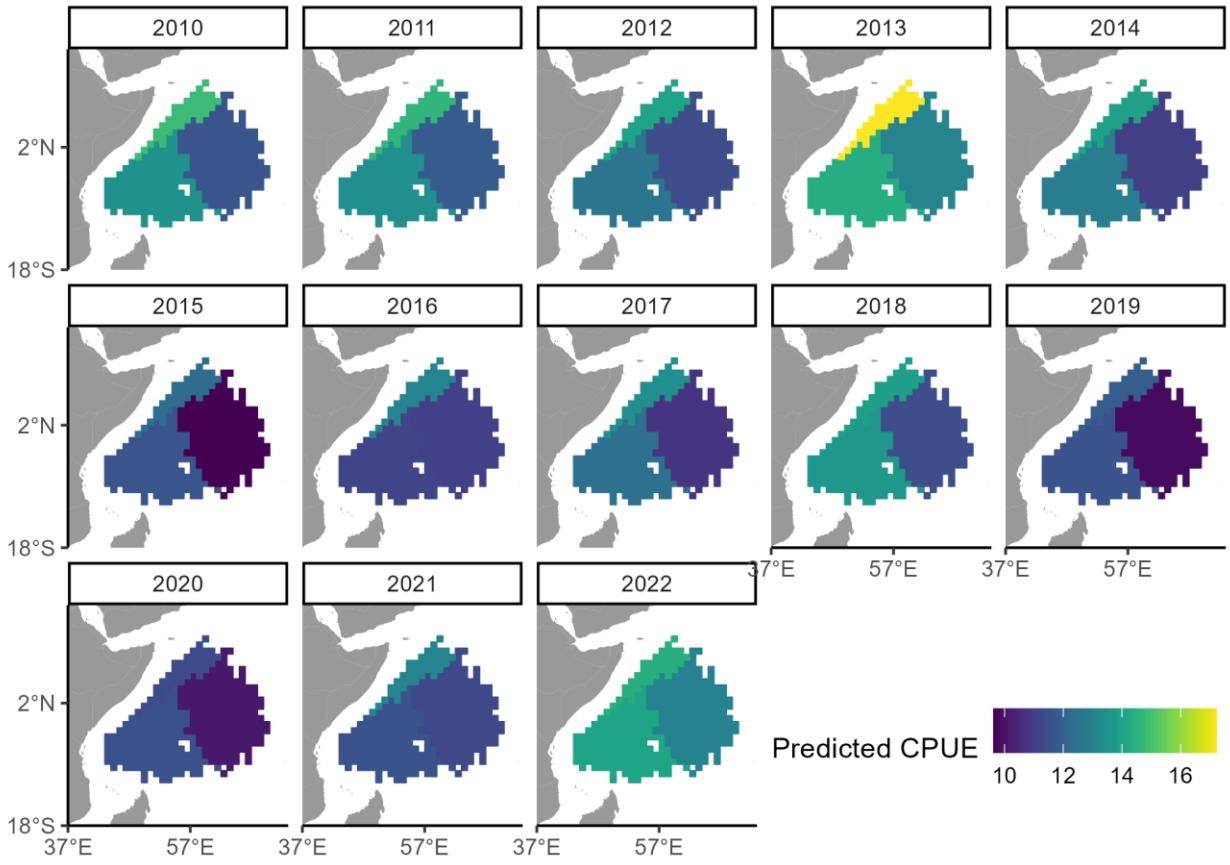

Figure 11: Predicted CPUE for each year-quarter-cluster combination by the GLMM model. Predicted values are aggregated by year.

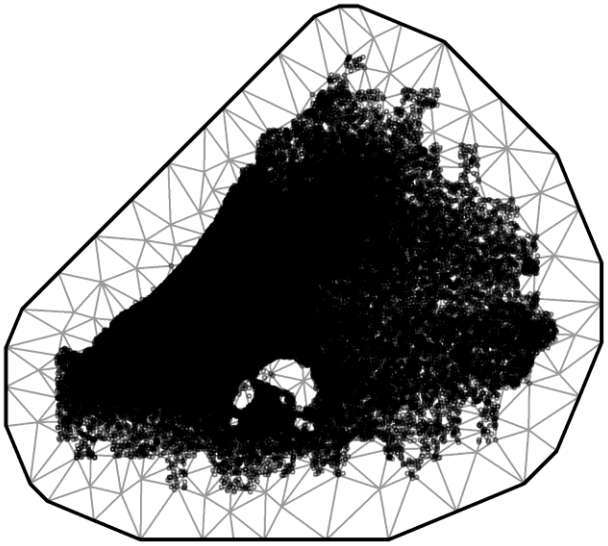

Figure 12: Mesh used in the spatiotemporal model (st-GLMM).

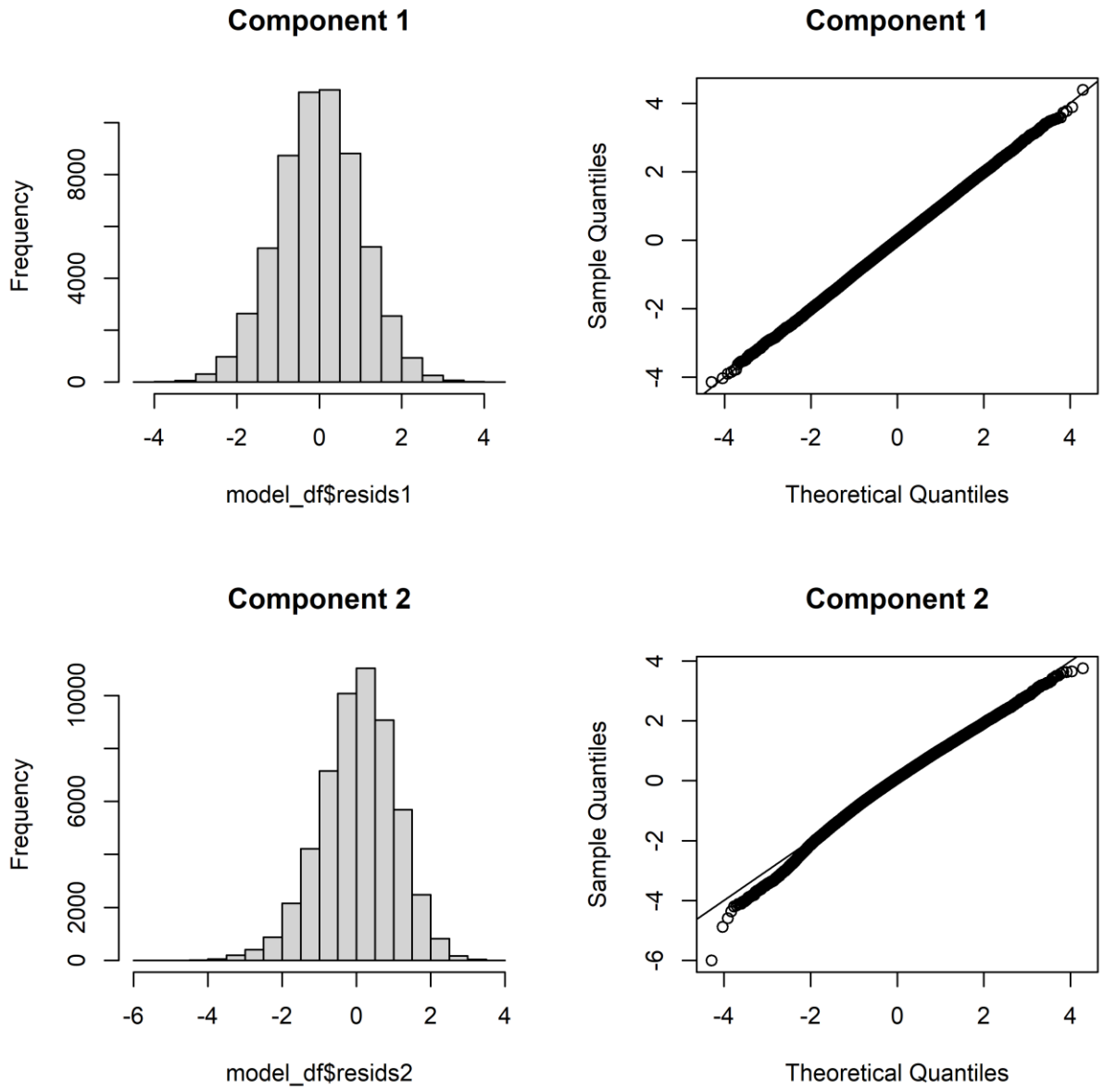

Figure 13: Residuals for each model componenet of the st-GLMM model.

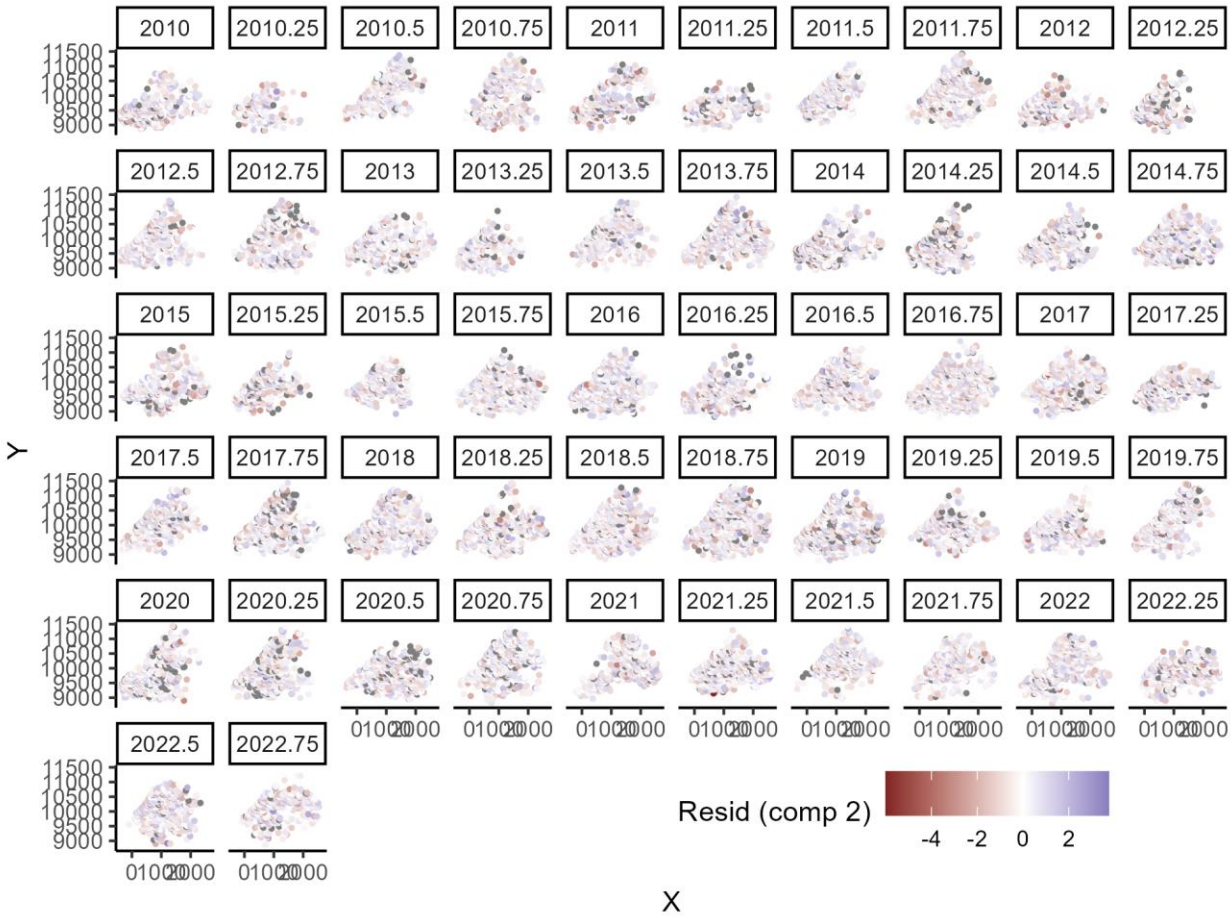

Figure 14: Spatial locations of residuals by time step (only shown for component 2) of the st-GLMM model.

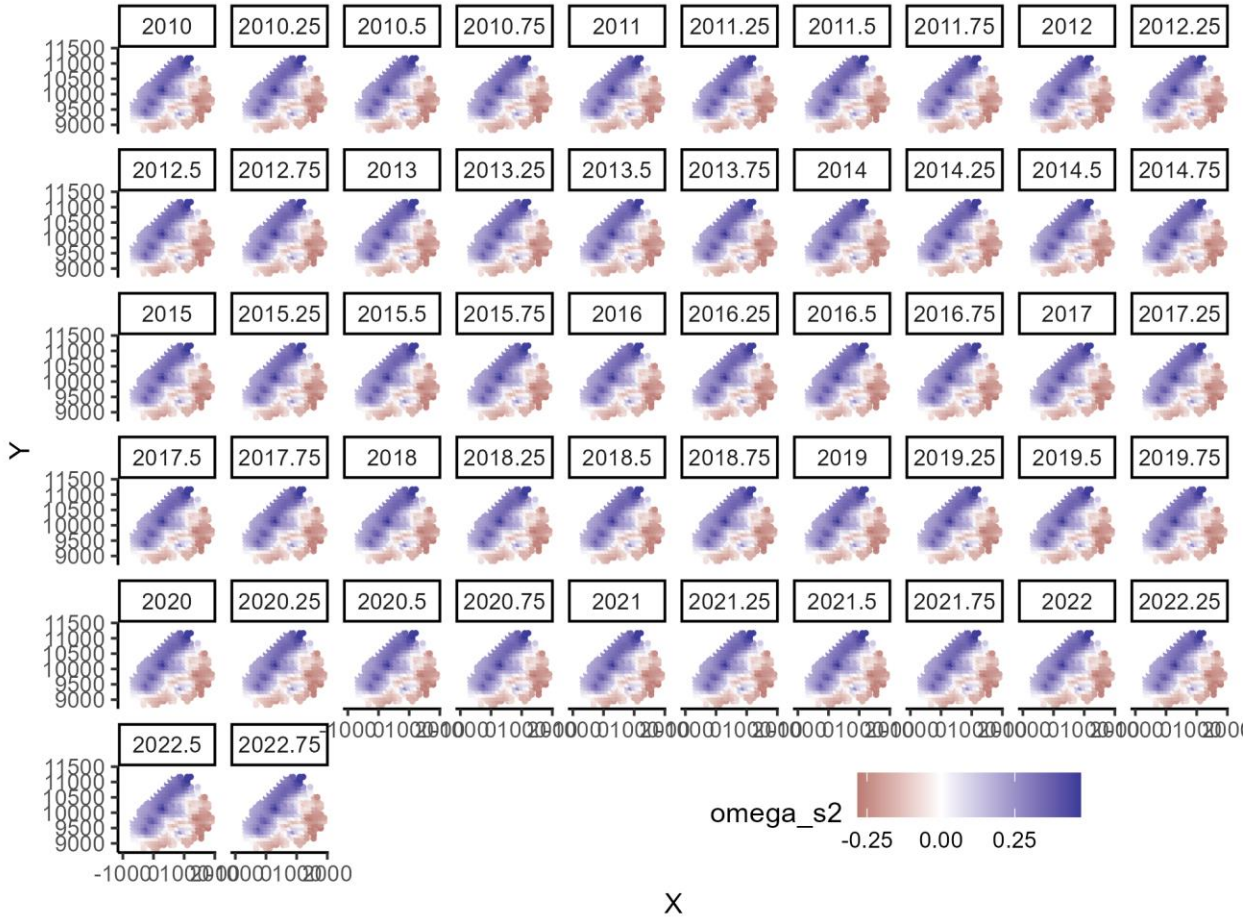

Figure 15: Estimated spatial effect for the second component of the st-GLMM model.

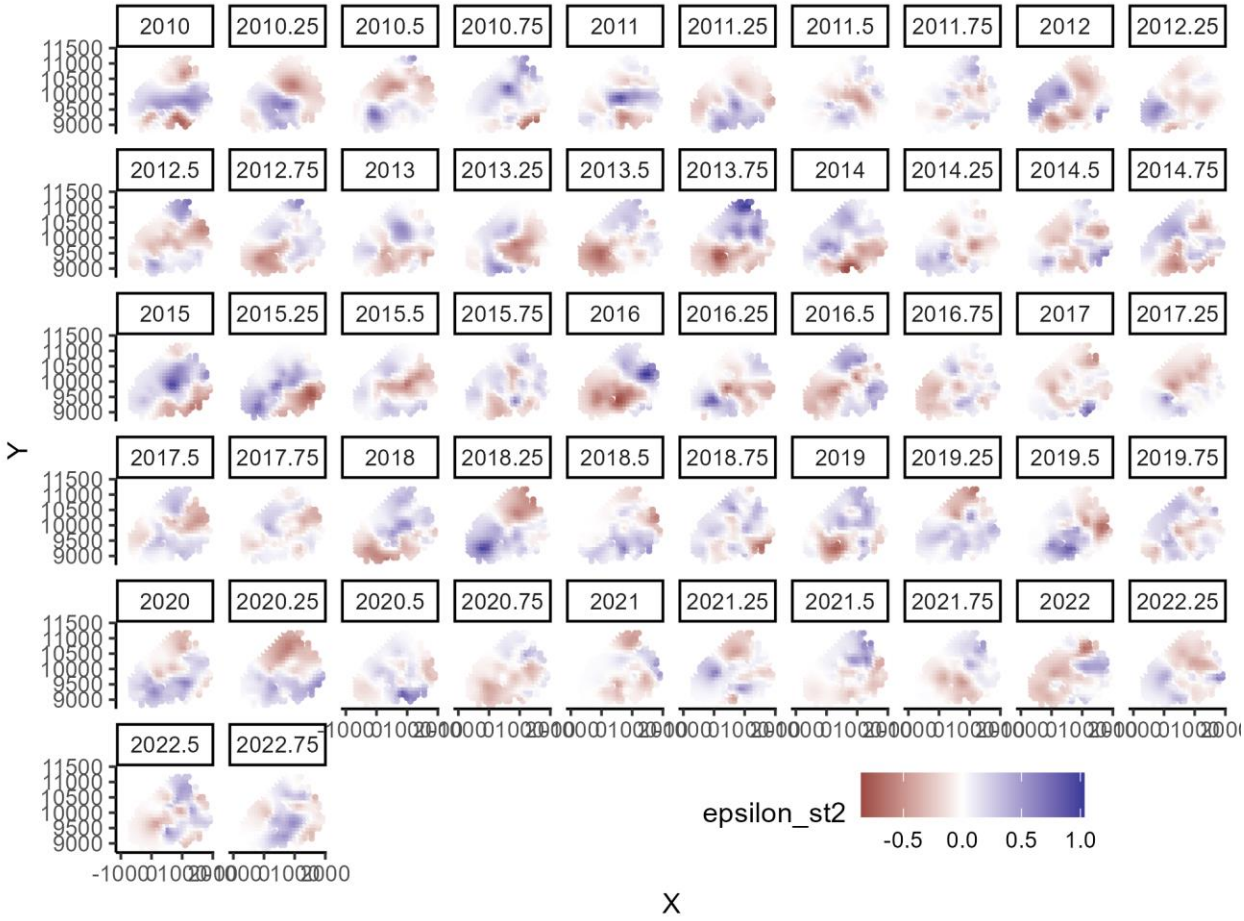

Figure 16: Estimated spatiotemporal effect for the second component of the st-GLMM model.

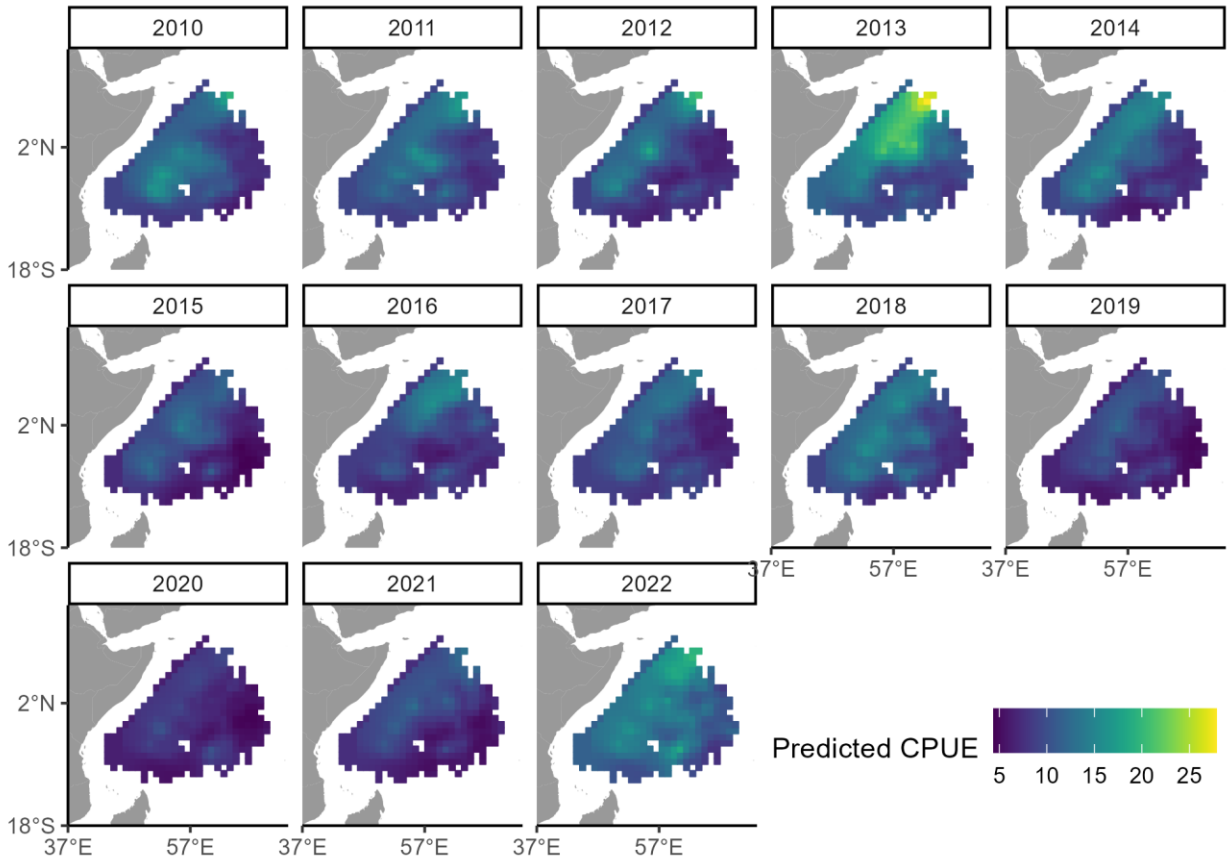

Figure 17: Predicted CPUE for each year-quarter-cluster combination by the st-GLMM model. Predicted values are aggregated by year.

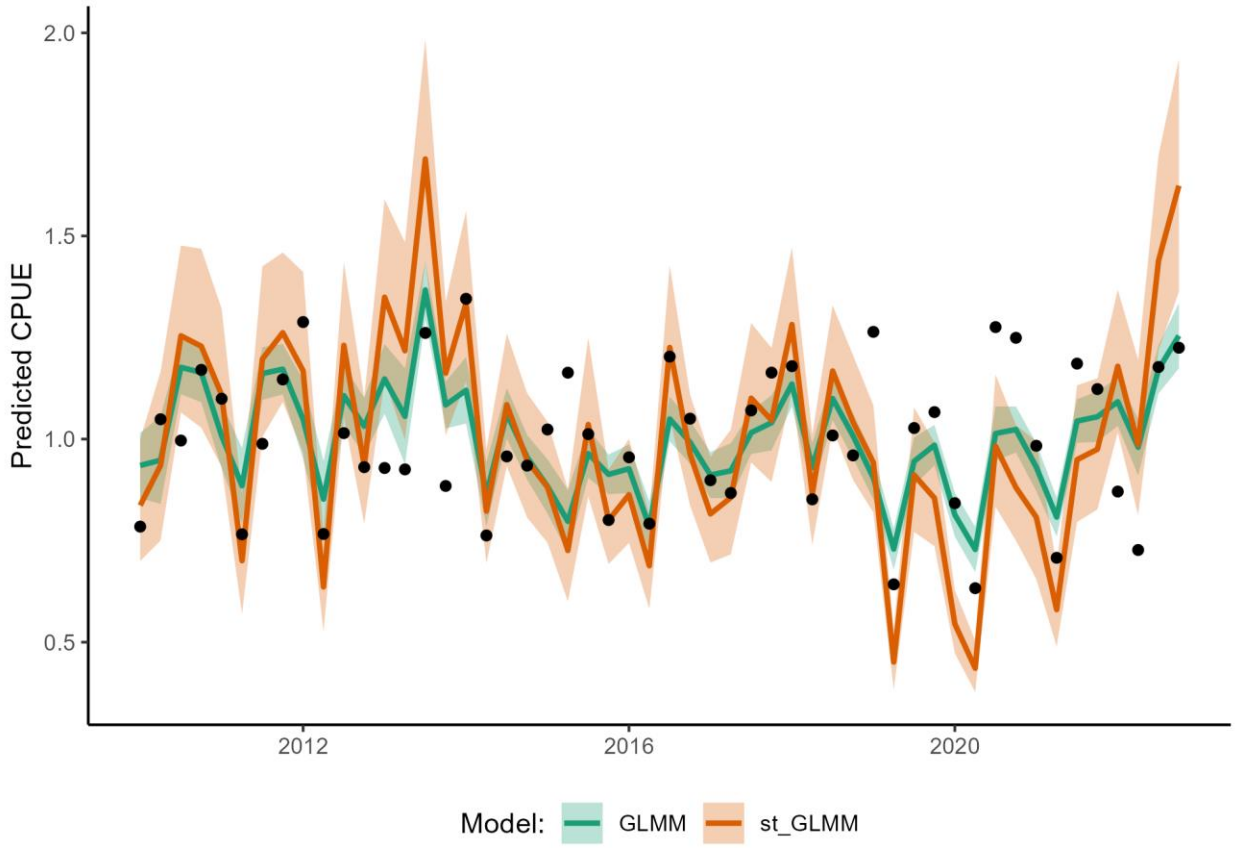

Figure 18: Predicted CPUE for year-quarter combination by the GLMM and st-GLMM models. The shaded area represents the 95% confidence interval. Nominal CPUE is also shown as black dots and calculated as the average catch per set per time step.

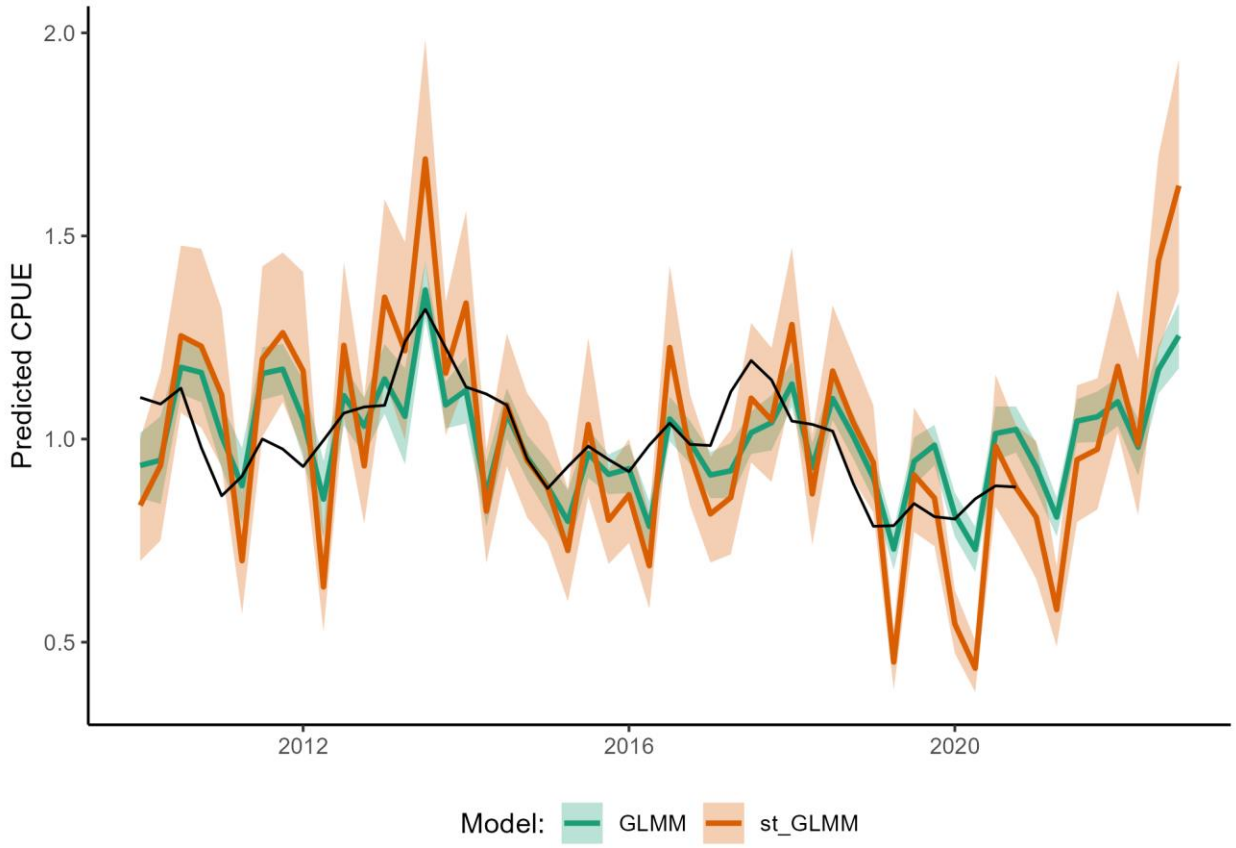

Figure 19: Predicted CPUE for year-quarter combination by the GLMM and st-GLMM models. The shaded area represents the 95% confidence interval. The vulnerable biomass to the PS log-school fishery estimated in the 2021 assessment model is also shown (black line).